ELSEVIER

Earth-Science Reviews 37 (1994) 89–134

EARTH-SCIENCE REVIEWS

Review: the atmospheric boundary layer

J.R. Garratt

CSIRO Division of Atmospheric Research, Private Bag No. 1, Mordialloc, Victoria 3195, Australia

Received 28 December, 1993; revised and accepted 27 April, 1994

Abstract

An overview is given of the atmospheric boundary layer (ABL) over both continental and ocean surfaces, mainly from observational and modelling perspectives. Much is known about ABL structure over homogeneous land surfaces, but relatively little so far as the following are concerned, (i) the cloud-topped ABL (over the sea predominantly); (ii) the strongly nonhomogeneous and nonstationary ABL; (iii) the ABL over complex terrain. These three categories present exciting challenges so far as improved understanding of ABL behaviour and improved representation of the ABL in numerical models of the atmosphere are concerned.

1. Introduction

1.1. Role of the atmospheric boundary layer

The atmospheric (or planetary) boundary layer plays an important role in many fields, including air pollution, agricultural meteorology, hydrology, aeronautical meteorology, mesoscale meteorology, weather forecasting and climate. We can summarise just a few of the problems for which boundary-layer knowledge is important, as follows

(a) Urban Meteorology is associated with the low-level urban environment and air pollution, including air pollution episodes involving photochemical smog and accidental releases of dangerous gases. The dispersal of smog and low-level pollutants depends strongly on meteorological conditions. Of particular importance is information on the likely growth of the shallow mixed layer resulting from surface heating, and on the factors controlling the erosion and ultimate breakdown of this inversion.

(b) Control and Management of Air Quality is closely associated with the transport and dispersal of atmospheric pollutants, including industrial plumes. Processes of concern include turbulent mixing in the ABL, particularly the role of convection, photochemistry and dry and wet deposition to the surface. In this general area, research on atmospheric turbulence has a very important practical application, and local meteorology, including the role of mesoscale circulations (sea breezes, slope winds, valley flows) and the phenomenon of decoupling of the low-level flow and the large scale upper flow, is also of major relevance.

(c) Aeronautical Meteorology is concerned with boundary-layer phenomena such as low cloud, low-level jets and intense wind shear leading to high intensity turbulence, particularly for aircraft landing and take-off. In the case of low clouds

0012-8252/94$26.00
SSDI 0012-8252(94)00032-R

and low-level jets, factors affecting their formation, maintenance and dissipation are of great importance.

(d) Agricultural Meteorology and Hydrology are concerned with processes such as the dry deposition of natural gases and pollutants to crops, evaporation, dewfall and frost formation. The last three are intimately associated with the state of the ABL, with the intensity of turbulence and with the energy balance at the surface.

(e) Numerical Weather Prediction (NWP) and Climate Simulation based on dynamical models of the atmosphere depend on the realistic representation of the Earth's surface and the major physical processes occurring in the atmosphere. It has been said (Stewart, 1979) that no general circulation model is conceptually complete without the inclusion of boundary-layer effects, and that no prediction model can succeed without a sufficiently accurate inclusion of the influence of the boundary. The boundary layer affects both the dynamics and thermodynamics of the atmosphere. There are a variety of dynamic effects: more than a half of the atmosphere's kinetic energy loss occurs in the ABL (Palmen and Newton, 1969). Boundary-layer friction produces cross-isobar flow in the lower atmosphere, whilst boundary-layer interaction permits air masses to modify their vorticity. From the thermodynamic perspective, all water vapour entering the atmosphere by evaporation from the surface must enter through the ABL. Even the oceans are strongly influenced by the ABL, since it is through the boundary layer that they gain most of their momentum so influencing the oceanic circulation.

1.2. Turbulence

From both a climate and local weather perspective, the most important ABL processes that need to be parametrised in numerical models of the atmosphere are vertical mixing and the formation, maintenance and dissipation of clouds. Those land-surface properties that are potentially crucial to accurate climate simulation include albedo, roughness, moisture content and vegetation cover.

Over land in particular, the structure of ABL turbulence is strongly influenced by the diurnal cycle of surface heating and cooling, by the presence of clouds and by horizontal variability in surface properties. Neutral flow, in which buoyancy effects are absent, is readily produced in the wind tunnel, and may be closely approximated in the atmosphere in windy conditions with a complete cloud cover. The unstably-stratified ABL, or convective boundary layer (CBL), occurs when strong surface heating (due to the sun) produces thermal instability or convection in the form of thermals and plumes, and when upside-down convection is generated by cloud-top radiative cooling. In strongly unstable conditions driven by surface heating, the outer region of the boundary layer in particular is dominated by convective motions and is often referred to as the mixed layer. In contrast, the stably-stratified ABL occurs mostly (though not exclusively) at night, in response to surface cooling by long wave emission to space. The unstable ABL is characterized by a near-surface superadiabatic layer, and the stable ABL by the presence of a surface inversion.

1.3. Boundary-layer depth

The top of the boundary layer in convective conditions is often well defined by the existence of a stable layer (capping inversion) into which turbulent motions from beneath are generally unable to penetrate very far, though they may continually erode it, particularly where latent heat is released in rising elements of air. The height of this elevated stable layer is quite variable, but is generally below 2 to 3 km. The top of a convective boundary layer is well defined in Fig. 1 by the sharp decrease in aerosol concentration at a height of about 1200 m, and coincides with the base of a deep and intense subsidence inversion. Over deserts in mid-summer under strong surface heating the ABL may be as much as 5 km deep, and even deeper in conditions of vigorous cumulonimbus convection. In stable conditions, in contrast to the above, the boundary layer is not so readily identified, turbulence is much weaker than in the unstable case, and consequently the depth no more than a few hundred metres at most. At night over land, under clear skies and light winds,

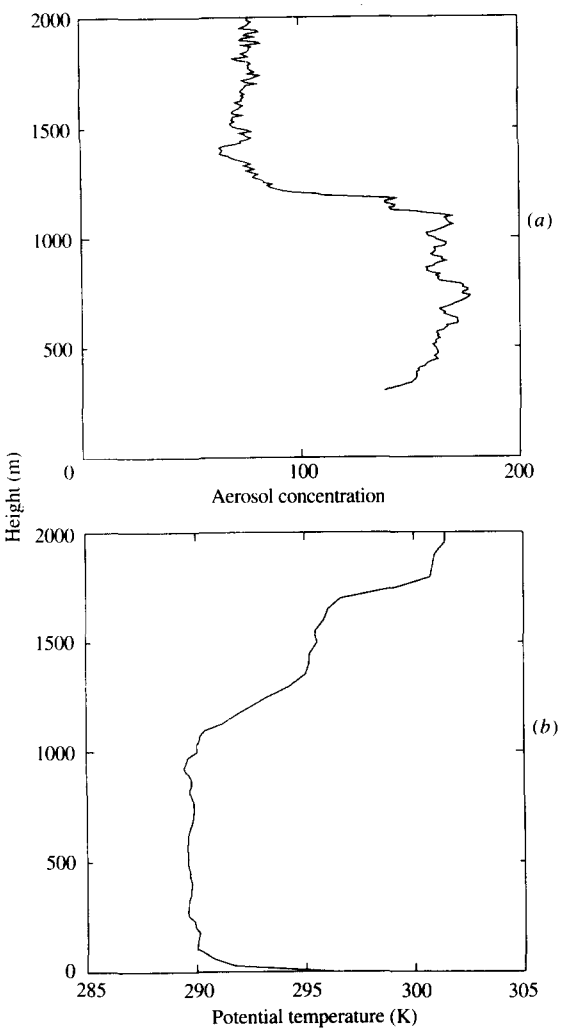

Fig. 1. Vertical profiles of (a) aerosol concentration in arbitrary units and (b) potential temperature observed overland in convective conditions (see Garratt, 1992; fig. 1.2).

it may be even smaller, perhaps no more than 50–100 m and strongly influenced by internal wave motions.

Over the open oceans, where low-level layer cloud (stratus and stratocumulus) is prevalent, the ABL depth may be no more than a few hundred metres and, in extratropical latitudes, may have a structure quite similar to that over land. According to results from the north-east Atlantic (the JASIN experiment — Businger and Charnock, 1983), the stability is near-neutral, with a capping stratocumulus layer and a depth on the order of 0.5 km. Such a shallow boundary layer is also found in coastal regions when warm air flows from land over a relatively cool sea. In the tropics, the mean structure is very much dependent on the season, and whether conditions are disturbed (in the vicinity of the inter-tropical convergence zone) or undisturbed. In the former, developing cumulus clouds result in poor definition of the ABL top, whilst in undisturbed conditions, the ABL top is well defined by the trade-wind inversion. Under special circumstances, the ABL depth over the ocean can be comparable to that over land in the middle of the day. This can occur during intense cold-air outbreaks over the ocean, when large "jumps" in temperature and humidity that identify the ABL top are particularly noticeable, and are the result of cold, dry air flowing out from the continent over relatively warm sea.

The purpose of this review paper is to provide the reader with an overview of boundary-layer structure and behaviour over land and sea (in the latter case, often cloud-topped), for homogeneous and heterogeneous surface conditions. In addition, some aspects of boundary-layer parametrisations for use in regional and global climate models are discussed. For more intensive reading, the classical texts should be consulted, e.g. Sutton (1953), Priestley (1959), Lumley and Panofsky (1964), Zilitinkevich (1970), Tennekes and Lumley (1972), Haugen (1973) and Brown (1974). Advanced texts dealing with specialised aspects of the ABL include Wyngaard (1980), Nieuwstadt and Van Dop (1982), Stull (1988), Sorbjan (1989) and Garratt (1992). For a general overview up to the late seventies consult McBean et al. (1979), and for a comprehensive introduction to instruments and techniques for making measurements in the ABL see Lenschow (1986). In recent times, Hess (1992) reviewed aspects of observations and scaling of the ABL, with attention given to the analysis of observations based on a framework of similarity scaling. The treatment for inhomogeneous surfaces was particularly emphasised. Most recently, an up-to-date review of roll vortices in the ABL has appeared (Etling and Brown, 1993), following on from that by Brown (1980). Etling and Brown (1993) review

recent advances in our understanding of organised large eddies in the ABL and on their role in the vertical transport of momentum, heat, moisture and chemical trace substances within the lowest part of the atmosphere.

2. Observations

Much of our knowledge of the ABL can be related to observations of turbulent flows made both in the laboratory and in the atmosphere. Such observations are important for understanding ABL processes, for the validation of numerical models and for placing suitable constraints on the behaviour of models.

Investigation of the structure of the lower part of the ABL has mainly utilized sensors located on tower structures. These towers have ranged in size from relatively short masts of a few metres height, to the 200–300 m tall structures that may support a very comprehensive suite of instrumentation. For studies of the whole boundary layer, early approaches had to rely on balloon-borne instrumentation — free and tethered sounding balloons, or constant volume free balloons — until aircraft techniques and facilities became more widely available.

For measurements throughout the ABL, the aircraft is now a well-established observational platform, although balloon platforms have been used with some success. One of the major advantages of using aircraft as an atmospheric measurement system is their mobility and capacity for making extended line averages of turbulent quantities (most aircraft flights occur at speeds of about 80 m s^{-1}). It can be used for both vertical profiling well above the tower layer, and for horizontal traverses. In many field experiments the two are combined. The main disadvantage of aircraft measurements is the need to measure accurately the aircraft motion, since corrections to the velocity and temperature measurements must be made for this motion.

In the last decade or so, ABL observations have been enhanced by remote sensing techniques. The newest instrumentation includes, for example, a range of sodars (acoustic sounders), lidars (light radars) and a range of Doppler radars. These mainly involve transmitted acoustic, light or radio energy, and the detection of the scattered energy due to (i) natural or artificial atmospheric targets (dust, salt, rain) as in Doppler radars and lidars; (ii) clear air refractive index fluctuations, as in acoustic sounders and FM-CW radars. All of the above techniques are called active, since they involve transmission of acoustic or electromagnetic radiation to the region of interest and measuring the backscattered fraction that is returned to the instrument. In contrast, passive techniques involve the measurement of radiation naturally emitted from the atmosphere, e.g. as in infrared radiometry.

Remote sensing techniques are attractive where in situ methods will not work or are uneconomical, and where the atmosphere interacts with the transmitted or received radiation allowing the meteorological variable of interest to be measured. Remote sensing utilises spatial averages, usually over volumes, and so is especially suitable if spatial averages are desired.

A brief summary of important field experiments may be of interest to the reader. In the early 1950's, the Scilly Isles field experiment of Sheppard et al. (1952) focussed on vertical momentum transfer processes over the ocean in the Northern Hemisphere westerlies. Major land-based ABL experiments commenced with the U.S. Great Plains observations in 1953 (Lettau and Davidson, 1957), followed by the Australian Wangara (Clarke et al., 1971) and Koorin (Clarke and Brook, 1979) observations in 1967 and 1974 respectively, and by the U.S. Minnesota experiment in 1973 (Izumi and Caughey, 1976). Interspersed with the above were the surface-layer experiments of Swinbank and co-workers in the 1960's at Hay and Kerang in southern Australia (Swinbank, 1968), and the Kansas experiment in 1968 (Izumi, 1971). Major international efforts with a strong ABL focus include BOMEX in 1969 (Kuettner and Holland, 1969), GATE in 1974 (Kuettner and Parker, 1976), AMTEX in 1974 and 1975 (Lenschow and Agee, 1976), and JASIN in 1978 (Charnock and Pollard, 1983) — all relating to the ABL over the ocean — HAPEX in 1986 (Andre et al., 1986) and FIFE in 1987

(American Meteorological Society, 1990). In Stull (1988), a list of major ABL field experiments can be found with associated references.

There have commenced or are planned a number of major international land-surface/ABL experiments with emphasis on the mesoscale (see Shuttleworth, 1991 for details). Of those completed, HAPEX-Mobilhy and FIFE are probably best known, whilst EFEDA took place in central Spain in 1991. There are several other experiments affiliated to the International Satellite Land Surface Climatology Program (ISLSCP). Of those planned or recently commenced, HAPEX-Sahel in Africa (1992) and BOREAS in Canada (1994) are the most noteworthy (see ISLSCP, 1993).

3. Theoretical framework

3.1. Basic equations

The presence of clouds leads to considerable complications compared to a dry ABL because of the important role played by radiative fluxes and phase changes. In a dry ABL, the turbulent structure, the mean variables and their evolution in time are controlled by the large-scale external conditions and by the surface fluxes. In a cloudy ABL, the surface fluxes may be important, but radiative fluxes produce local sources of heating or cooling within the interior of the ABL and therefore can greatly influence its turbulent structure and dynamics. The state of equilibrium of a cloud-topped boundary layer (CTBL) is determined by competition between radiative cooling, entrainment of warm and dry air from above the cloud, large-scale divergence and turbulent buoyancy fluxes. The phase change of water in a cloudy ABL introduces, in addition to Θ_v and q, a third variable in the form of the liquid water content q_l (refer to the Table of symbols for explanation). In the presence of liquid water clouds within the ABL, equations for mean temperature and water variables must take into account the possibility of phase changes, and include a conservation equation for mean liquid water content (either as a specific humidity or mixing ratio).

For the non-homogeneous ABL, horizontal variations of properties in the ABL may arise from non-uniform surface features (z_0, T_0 variations due to soil moisture, albedo, land-water contrast) or in the presence of orography, and be associated with thermally forced mesoscale circulations (e.g. sea breezes), internal boundary layers (at the coast) and slope flows. Important terms to be included in a mathematical description of the ABL are those describing advection, e.g. in the 2D system, terms such as $u\partial/\partial x$ and $w\partial/\partial z$.

For ease of discussion, we limit ourselves to the 2D case, and start with the equations for the set of mean field quantities (u, v, Θ_v, q, q_l) most relevant to the cloudy, 2D ABL. The five basic prognostic equations are, in scalar form,

$$\partial u/\partial t + u\partial u/\partial x + w\partial u/\partial z = -\rho^{-1}\partial p/\partial x + fv - \partial(\overline{u'w'})/\partial z \quad (1)$$

$$\partial v/\partial t + u\partial v/\partial x + w\partial v/\partial z = -\rho^{-1}\partial p/\partial y - fu - \partial(\overline{v'w'})/\partial z \quad (2)$$

$$\partial\theta_v/\partial t + u\partial\theta_v/\partial x + w\partial\theta_v/\partial z = (\rho c_p)^{-1}\partial R_N/\partial z - \partial(\overline{w'\theta_v'})/\partial z - \lambda M/\rho c_p \quad (3)$$

$$\partial q/\partial t + u\partial q/\partial x + w\partial q/\partial z = -\partial(\overline{w'q'})/\partial z + M/\rho \quad (4)$$

$$\partial q_l/\partial t + u\partial q_l/\partial x + w\partial q_l/\partial z = -\partial(\overline{w'q_l'})/\partial z + W_q/\rho - M/\rho. \quad (5)$$

Here, M is the mass of water vapour per unit volume per unit time being created by a phase change from liquid or solid, and W_q is a net liquid water source/sink term (e.g. it is negative for net precipitation leaving the air parcel). The turbulence terms of the form $\partial\overline{w's'}/\partial z$ are of the greatest importance in the ABL and represent the effects of small-scale turbulent mixing on the mean fields. Additional equations required to close the set include the gas equation, the continuity equation, and possibly a turbulent kinetic energy (TKE) equation relevant to the turbulence closure, viz.

$$\partial e/\partial t + u\partial e/\partial x + w\partial e/\partial z = -\overline{u'w'}\partial u/\partial z - \overline{v'w'}\partial v/\partial z + (g/\theta_v)\overline{w'\theta_v'} - \partial(\overline{w'e} + \overline{w'p'}/\rho)/\partial z - \epsilon \quad (6)$$

where e is the mean TKE ($e = \overline{u'^2} + \overline{v'^2} + \overline{w'^2}$) and ϵ is the molecular rate of dissipation of TKE. Note that on the RHS of Eqs. 1 to 5 $\partial/\partial x$ terms in turbulent quantities are neglected (this is an excellent assumption for horizontal length scales $\gg$ vertical scales). We can reduce this set so as to simplify the equations if we confine the problem to a (i) clear, 2D, (ii) clear, 1D (homogeneous) ABL. The following simplifications can be made when not dealing with the cloudy, 2D ABL: (i) in the clear case, $q_l = M = W_q = 0$; (ii) in the 1D case, $\partial/\partial x = w = 0$.

The above equations provide a sound framework for study of the physical aspects of the ABL, and of its modelling. In solving the set Eqs. (1)–(6), considerable attention must be given to the closure problem — this involves parametrisation of the covariance or higher-order terms. In addition, two options so far as ABL study is concerned are generally available (see Clarke, 1970; Deardorff, 1972), (i) the requirement for internal structure, hence the height variation of mean and turbulent quantities; (ii) treating the ABL as a slab, of variable height h. In both, the behaviour and knowledge of surface fluxes is an important requirement.

3.2. Surface fluxes and profile relations

The surface values of the covariances are of particular importance, both as a basis for scaling purposes and as lower boundary conditions for solution of Eqs. (1)–(5). The surface fluxes define a set of turbulent scaling parameters used in Monin–Obukhov theory as follows: $u^2_{*o} = [(\overline{u'w'})^2_o + (\overline{v'w'})^2_o]^{1/2} = -(\overline{u'w'})_o$ if surface-wind coordinates are used, with $v = 0$. Here, u_{*o} is the surface friction velocity. Temperature and humidity scales, Θ_{*o} and q_{*o} are defined by $\Theta_{*o} = -(\overline{w'\Theta'_v})_o/u_{*o}$ and $q_{*o} = -(\overline{w'q'})_o/u_{*o}$, with a stability length scale L (the Obukhov length) defined by $L = u^2_{*o}\Theta_v/(kg\Theta_{*o})$ with k the von Karman constant. The above scaling applies in neutral, moderately unstable and stable conditions, but in highly convective conditions, particularly well away from the surface, mixed-layer or free convection scales for velocity, w_*, and temperature, T_*, are used where $w^3_* = g(\overline{w'\Theta'_v})_o h/\Theta_v$ and $T^3_* = \Theta_v(\overline{w'\Theta'_v})^2_o/gh$ where h is the depth of the CBL. In highly stable conditions, well away from the surface ($z > L$), local scaling is more appropriate and relies on scaling turbulence properties using local flux values, not surface values.

With u_{*o} serving as an intrinsic internal velocity scale, suitable scaling of Eqs. (1) and (2) simplified to the clear, 1D case leads to the logarithmic wind law in neutral conditions (Tennekes, 1982), whilst Monin–Obukhov theory introduces the length scale L to take account of buoyancy effects. Thus, in the surface layer, over surfaces that are not too rough (typically, this implies values of the aerodynamic roughness length z_o no more than a few tens of centimetres) and at heights where $z/z_o \geqslant 10$–100 (e.g. Garratt, 1980, 1983),

$$(kz/u_{*o})\partial u/\partial z = \Phi_M(\zeta) \tag{7a}$$

$$(kz/\theta_{*o})\partial\theta_v/\partial z = \Phi_H(\zeta) \tag{7b}$$

or in integrated form,

$$ku/u_{*o} = \ln(z/z_o) - \Psi_M(\zeta) \tag{8a}$$

$$k(\theta_{va} - \theta_o)/\theta_{*o} = \ln(z/z_T) - \Psi_H(\zeta) \tag{8b}$$

where subscripts "a" and "o" refer to the air and surface respectively, and for humidity Eqs. (7b), (8b) apply, with Θ_v or Θ replaced by q, and z_T replaced by z_q. The functions $\Phi_{M,H}(\zeta)$, $\Psi_{M,H}(\zeta)$ are well known (Brutsaert, 1982; Garratt, 1992; see also Beljaars and Holtslag, 1991), but at lower heights ($z/z_o < 10$–100) within the roughness sublayer (sometimes called the transition layer), the Φ and Ψ profile functions must be modified (e.g. Garratt, 1980, 1983; Raupach et al., 1980). The details are not pursued here. In general, the roughness lengths z_o and z_T (or z_q) are not equal; discussions on their relative values can be found in Brutsaert (1982; ch. 4), Garratt (1992; ch. 4); also see, Garratt and Hicks (1973), Beljaars and Holtslag (1991), Betts and Beljaars (1993), Garratt et al. (1993) and Mahrt and Ek (1993).

The above equations form the basis of the bulk transfer relations for surface fluxes (τ_o is the

surface stress, H_o the surface heat flux and E_o is the surface evaporation), written as follows

$$\tau_o/\rho = -(\overline{u'w'})_o = u_{*o}^2 = C_D u^2 \quad (9)$$

$$H_o/\rho c_p = (\overline{w'\theta_v'})_o = -u_{*o}\theta_{*o} = C_H u(\theta_o - \theta_{va}) \quad (10)$$

$$E_o/\rho = (\overline{w'q'})_o = -u_{*o}q_{*o} = C_E u(q_o - q_a) \quad (11a)$$

$$= (q_o^* - q_a)/(r_s + r_a) \quad (11b)$$

where q^* is the saturated humidity, r_s is a surface resistance, the aerodynamic resistance $r_a = (C_E u)^{-1}$ and the coefficients C_D, C_H, C_E are readily deduced as functions of z/z_o and ζ from manipulation of Eqs. (7) and (8). By setting the Ψ functions to zero, the neutral values C_{DN}, C_{HN}, C_{EN} are also defined. In the above, surface-layer wind coordinates are used, so that u is the surface-layer (total) wind.

The above transfer relations can be written in terms of ABL-averaged quantities, incorporating ABL transfer coefficients (e.g. geostrophic drag coefficients). The result is (e.g. Garratt, 1992)

$$k\hat{u}_g/u_{*o} = k\hat{u}/u_{*o} = \ln(h/z_o) - A(\mu, M_x, R) \quad (12)$$

$$k\hat{v}_g/u_{*o} = k\hat{v}/u_{*o} - ku_{*o}/fh = -B(\mu, M_y, R)\,\mathrm{sign(f)} \quad (13)$$

$$k(\hat{\theta}_v - \theta_o)/\theta_{*o} = \ln(h/z_T) - C(\mu, \boldsymbol{M}, R) \quad (14)$$

$$k(\hat{q} - q_o)/q_{*o} = \ln(h/z_q) - D(\mu, \boldsymbol{M}, R) \quad (15)$$

which, in analogy with the surface-layer manipulation of Eqs. (7) and (8), leads to relations for the surface fluxes in terms of geostrophic or boundary-layer transfer coefficients (Garratt, 1992; ch. 3). Here, $\boldsymbol{M}$ is a baroclinity parameter whose magnitude is defined as $|\boldsymbol{M}|^2 = M_x^2 + M_y^2$, $\mu = h/L$ and $R = |f|h/u_{*o}$. Variables with the circumflex are vertical averages. Functional forms for the A, B, C and D can be found in the literature (Brutsaert, 1982; Garratt, 1992), with Fig. 2 showing the ABL drag coefficient and cross-isobar flow angle (from Eqs. 12 and 13) as functions of h/z_o and μ. Note that these curves strongly reflect observations since the functions A and B are directly inferred from these for a range of experiments.

Recently, Walmsley (1992) has proposed a new ABL resistance law for neutrally-stratified flow which, in essence, has strong similarities to that generally accepted. However, comparison against observations reveals no significant improvement to the geostrophic drag law as represented by Eqs. (12) and (13).

3.3. Vertical variation of fluxes and the K approach

The covariances (vertical fluxes) can be parametrised as

$$\tau_x = -\rho\overline{u'w'} = \rho K_m \partial\overline{u}/\partial z \quad (16)$$

$$\tau_y = -\rho\overline{v'w'} = \rho K_m \partial\overline{v}/\partial z \quad (17)$$

$$H = \rho c_p \overline{w'\theta_v'} = -\rho c_p K_H \partial\overline{\theta}_v/\partial z \quad (18)$$

$$E = \rho\overline{w'q'} = -\rho K_W \partial\overline{q}/\partial z \quad (19)$$

where K_M is the eddy viscosity, K_H the eddy thermal diffusivity and K_W is the eddy diffusivity for water vapour. In contrast to the molecular case, the eddy diffusivity is not a property of the fluid but may be a function of many quantities, including position and flow velocity. Here simple forms for K may be used (e.g Garratt, 1992; ch. 8), or calculated by consideration of the TKE equation (Eq. 6) with $K \propto e^{1/2}l$, l being a mixing length. Alternatively for numerical purposes, we can carry equations for the covariances themselves (second-order closure).

For modelling purposes, vertical fluxes of momentum, heat and water vapour and other scalars can be evaluated using either local or non-local closure schemes. It is apparent that convective mixed-layer turbulence is one of the more difficult regimes to model using local closure, because the important eddy length scales are comparable with the thickness of the CBL. Rather, the validity of K-theory and mixing length assumptions requires eddies that are much smaller than the scale of interest. In the presence of large eddies and intense mixing, the CBL can often be assumed to be well-mixed, though on some occa-

sions over land and sea it is distinctly unmixed in one or more of the properties. This lack of mixing is apparent in the profiles of potential temperature and specific humidity shown in Fig. 3.

The application of K-theory to the Θ_v profiles in particular has obvious limitations, since the heat flux may often appear to be countergradient on average, and therefore will require K to be

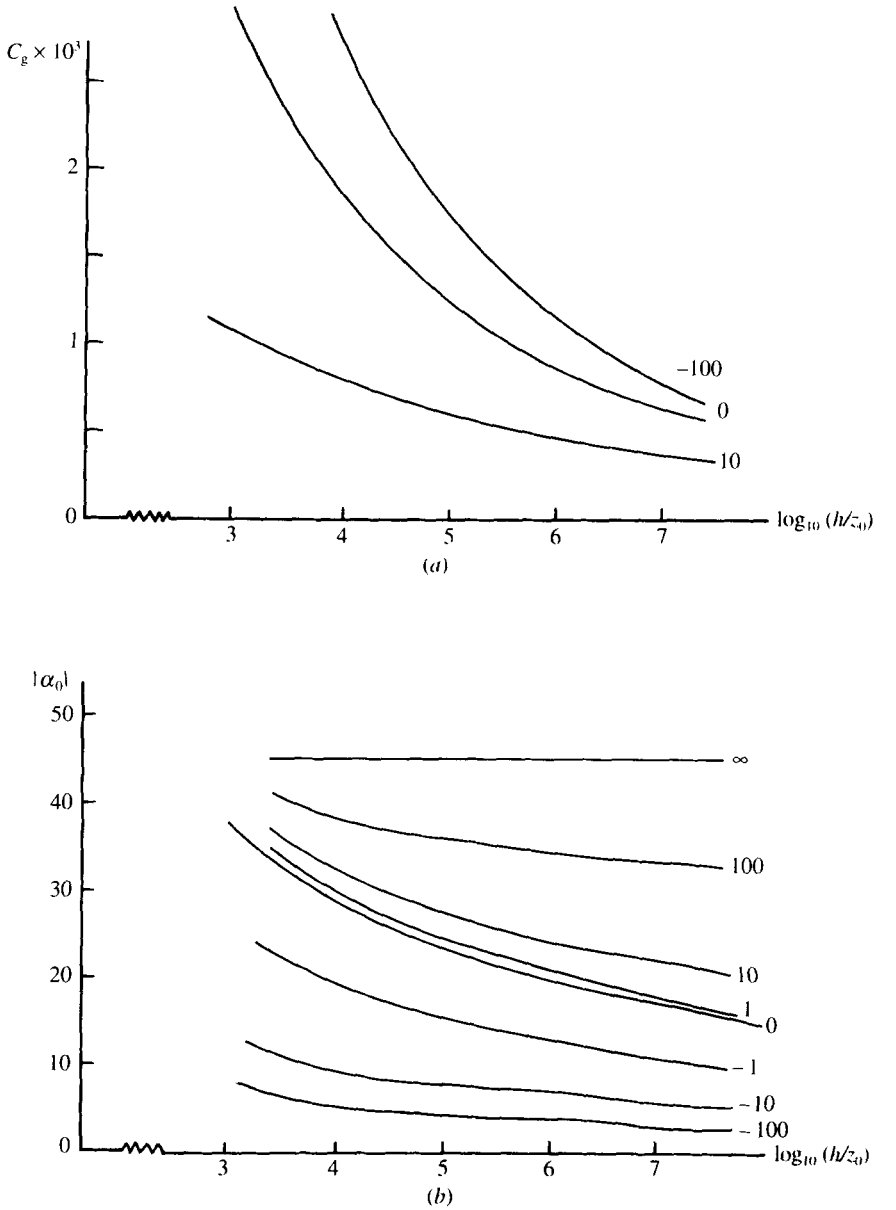

Fig. 2. Variations of (a) the boundary-layer drag coefficient (C_g) and (b) cross-isobar flow angle (α_o) as functions of h/z_o and stability parameter μ (negative μ corresponds to unstable conditions) — see Eqs. (12) and (13). Here $C_g = u_{*o}^2/(u_g^2 + v_g^2)$ and $\tan(\alpha_0) = v_g/u_g$. See Garratt (1992; fig. 3.12).

negative, and in parts of the profile (in mid-regions of the CBL usually) may even be singular. The nature of the scalar mean profiles in the CBL determines whether local closure will be appropriate. The presence of entrainment profoundly influences the mean temperature and scalar mixing ratio profiles (Θ_v and q, for example) through what is referred to as "top-down diffusion". This type of diffusion differs from the familiar "bottom-up" diffusion because the buoyant forcing of the convective turbulence occurs with vertical asymmetry. Numerical simulations reveal that the flux-gradient relationship (involving an eddy diffusivity) for a passive scalar in a mixed layer depends on the boundary from which the flux originates (e.g. Wyngaard and Brost, 1984). To see this, and how it relates to the K problem, consider a passive, conservative scalar whose mean concentration c satisfies

$$\partial c/\partial t = -\partial(\overline{w'c'})/\partial z \tag{20}$$

where $\overline{w'c'}$ is the scalar flux. If temporal changes in the scalar gradient $\partial c/\partial z$ are assumed negligible then the flux profile is linear, and described by

$$\overline{w'c'} = (\overline{w'c'})_o(1 - z/h) + (\overline{w'c'})_h(z/h) \tag{21}$$

so that the flux at any level has contributions from bottom-up (through $(\overline{w'c'})_o$) and top-down diffusion (through $(\overline{w'c'})_h$).

If we associate eddy diffusivities K_b and K_t with bottom-up and top-down diffusion respectively, then it is readily shown under the assumption of superposition of properties that

$$\partial c/\partial z = -\left((\overline{w'c'})_o(1 - z/h)/K_b + (\overline{w'c'})_h(z/h)/K_t\right) \tag{22}$$

which shows that

(a) If both fluxes are of the same sign, the vertical gradient of c will tend to be large — this is characteristic of the humidity profile.

(b) If the fluxes are of opposite sign, the vertical gradient may be close to zero — this occurs with the temperature profile.

We also have for K, using Eq. (22),

$$K = -\overline{w'c'}/(\partial c/\partial z) = \frac{K_b K_t \overline{w'c'}}{K_t(\overline{w'c'})_o(1 - z/h) + K_b(\overline{w'c'})_h(z/h)}. \tag{23}$$

Since K depends on the fluxes, this shows that the closure is inherently non-linear with $0 < K < \infty$. The poor behaviour in K can occur even when

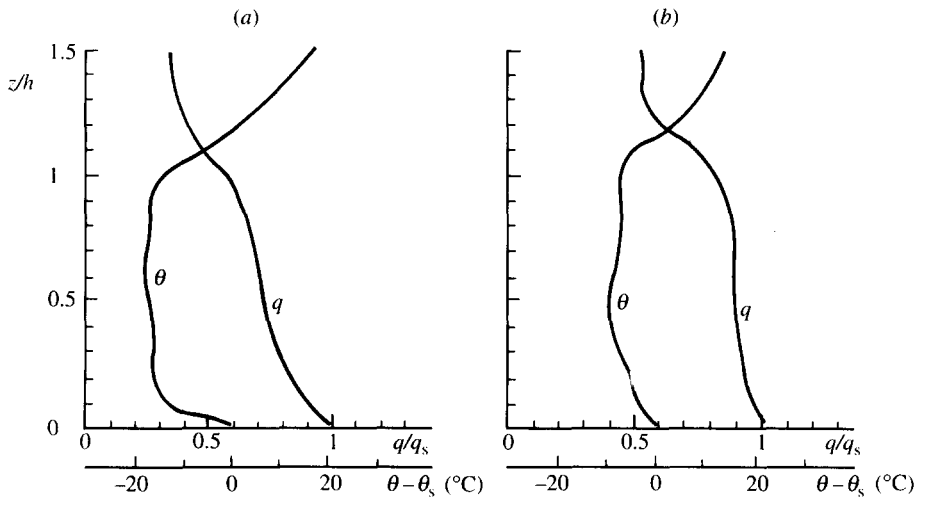

Fig. 3. Mean Θ and q profiles in unstable conditions in (a) Colorado and (b) south-eastern Australia; in (a) ABL height $h = 1710$ m and in (b) $h = 915$ m. Subscript s denotes "screen-level" values. After Mahrt (1976).

K_b and K_t are well-behaved, but different (see Holtslag and Moeng, 1991).

For the determination of the c profile, Eq. (22) requires knowledge of the eddy diffusivities before integration can be made. The form of the diffusivities has been obtained from large-eddy simulations (e.g. Moeng and Wyngaard, 1984; Holtslag and Moeng, 1991), with $K_t = 1.4\, w_* z(1 - z/h)^2$ and $K_b = w_* h(1 - z/h)/g_b$. The top-down diffusivity is well-behaved and positive throughout the convective boundary layer. In contrast, the mean gradient function g_b is positive in the lower regions of the mixed layer and near the surface, but changes sign near $z/h = 0.6$ and is negative above (Moeng and Wyngaard, 1984). This is a clear illustration of the breakdown of the K_b model, with K having a singularity in the mid-regions of the mixed layer. The result for K shows that the bottom-up process generates a countergradient flux in the upper mixed layer.

With suitable bottom boundary conditions, the c profile for various values of the ratio $R = (\overline{w'c'})_h/(\overline{w'c'})_0$ is shown in Fig. 4. Small negative R values give a profile form similar to that for potential temperature (e.g. with $R = -\beta = -0.2$) and illustrate the countergradient heat flux problem in the upper regions of the CBL. Positive R values yield distinctly "unmixed" profiles, as occurs with humidity at times.

Local closure has problems because it relates the flux of a quantity at a given level to properties at that level. The alternative approach uses non-local closure, either in the form of a non-local K (e.g. Holtslag and Moeng, 1991; also see Holtslag and Boville, 1993) as discussed above or in the form of integral (e.g. Fiedler, 1984) or transilient methods (Stull, 1984, 1993; Stull and Driedonks, 1987).

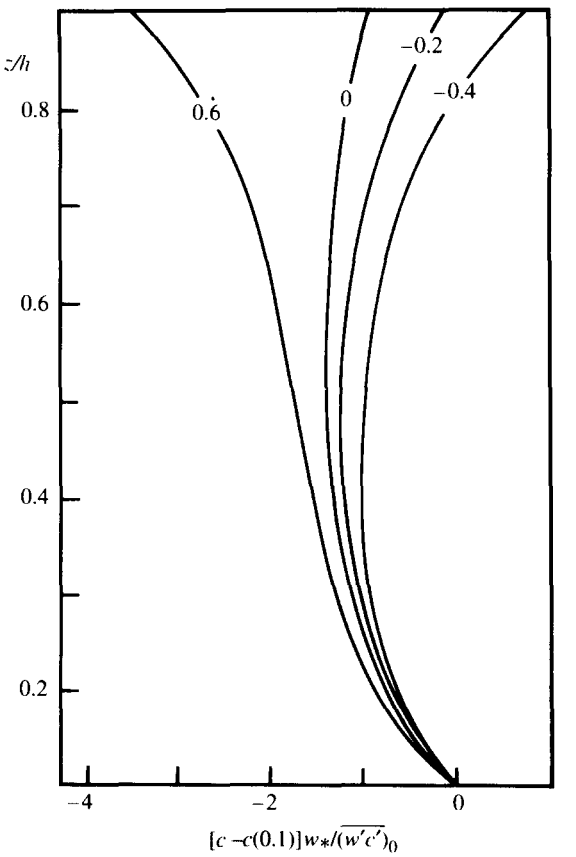

Fig. 4. Scaled concentration profiles for four values of the parameter R — see Garratt (1992; fig. 6.10). Here $c(0.1)$ is the concentration at $z/h = 0.1$, calculated from the integrated form of Eq. (22).

3.4. Slab approach and rate equation for ABL depth

Where the ABL is treated as a slab, of depth h, vertical integration of Eqs. (1)–(4) in the 1D non-cloudy case leads to equations for the slab velocity, temperature and humidity. This can be illustrated for temperature, where,

$$\partial\hat{\theta}_v/\partial t = \left[(\overline{w'\theta'_v})_0 - (\overline{w'\theta'_v})_h\right]/h. \qquad (24)$$

This, and other analogous equations for slab properties, contain entrainment fluxes at h. These can be formally related to the jumps at $z = h$, (e.g. $\Delta\Theta_{vh}$ for virtual potential temperature) so that for heat transfer,

$$(\overline{w'\theta'_v})_h = -\Delta\theta_{vh}(\partial h/\partial t - w_h). \qquad (25)$$

Here the mean vertical velocity at $z = h$ is represented by w_h.

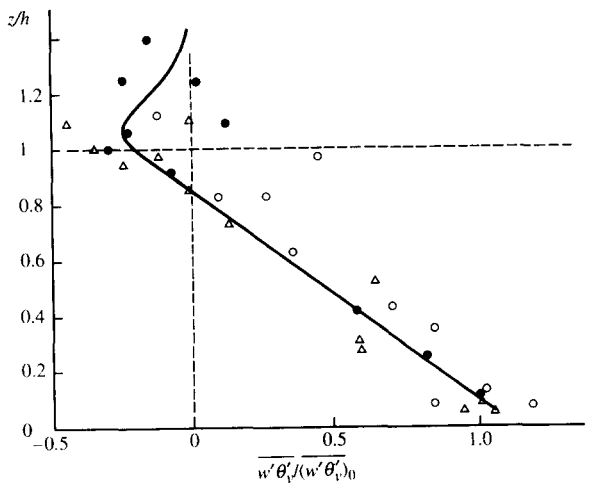

Fig. 5. Vertical variation of the normalised sensible heat flux based on experimental data from aircraft — see Garratt (1992; fig. 6.2).

As the slab properties change, so do the respective jumps across the top of the CBL. In the case of temperature, this is given by

$$\partial(\Delta\theta_{vh})/\partial t = \gamma_\theta(\partial h/\partial t - w_h) - \partial\theta_{vm}/\partial t, \qquad (26)$$

where γ_θ is the vertical Θ gradient above h. Eqs. (24)–(26) need to be solved for h and Θ_{vm}; if we assume w_h and γ_θ are given, and the surface heat flux is specified, closure is achieved by relating the entrainment heat flux to that at the surface. Such a relationship may be based on the TKE equation (e.g. see Manins, 1982), and usually leads to the simple form $(\overline{w'\Theta_v'})_h = -\beta(\overline{w'\Theta_v'})_o$. Observations above surfaces of low roughness suggest that in convective conditions $\beta \approx -0.2 \pm 0.1$ (Stull, 1988, ch. 11 — see also Manins, 1982), with tentative evidence of values closer to -0.5 over large roughness surfaces (e.g. Clarke, 1990). The observed heat-flux profiles in Fig. 5 are consistent with the low-roughness value of -0.2, and model results tend to confirm this too (e.g. Nieuwstadt et al., 1993 for LES models; Chrobok et al., 1992 for 1D and 2D boundary-layer models).

Expressions for h range from the simple encroachment-only form, where $\partial h/\partial t = (\overline{w'\Theta_v'})_h/\gamma_\theta h$, to the more detailed descriptions e.g. that of Deardorff (1974). Observed and simulated ABL growth under convective conditions are shown in Fig. 6, revealing the relative behaviour of a range of formulations.

Applications to the nocturnal boundary layer (NBL) are not so well developed, but the approach is equally as valid, except that h is differ-

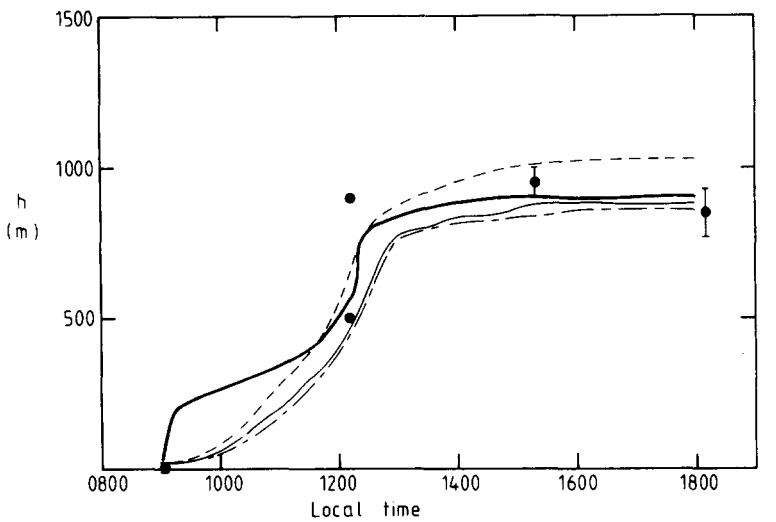

Fig. 6. Observed (•) and predicted ABL growth in unstable conditions — from Manins (1982). Predictions are from an encroachment model, with (— - —) and without (—) thermal wind; a flux-ratio closure model (— — —) and from a Froude dynamics model (———).

ent. A suitable rate equation was described by Nieuwstadt and Tennekes (1981),

$$\partial h/\partial t = -\Delta\theta^{-1}(h_e - h)\partial\theta_o/\partial t \quad (27)$$

where $\Delta\Theta$ is the temperature change from the surface to h, and h_e is the equilibrium height given by the Zilitinkevich (1972) relation;

$$h_e = \gamma_e(u_* L/|f|)^{1/2}. \quad (28)$$

This relation evolves naturally from scaling of the momentum equation, with the constraint of constant gradient Richardson number with height (Nieuwstadt, 1984).

4. Homogeneous continental abl

4.1. Surface-layer

Flux-gradient relations

Much observational evidence now exists in support of the Monin–Obukhov theory, and its breakdown in highly stable or unstable conditions. A summary of the multitude of Φ analytical expressions in both stable and unstable conditions can be found in table 4.2 of Sorbjan (1989). In the case of Φ_M and Φ_H over a wide unstable range, the observations presented in Kader and Yaglom (1990; fig. 1) confirm Monin–Obukhov predictions and the approach to free convective behaviour — see Fig. 7. Any of these gradient functions can be used to infer the stability functions in Eq. (8) and thus the stability dependences of the transfer coefficients in Eqs. (9)–(11). The reader should also refer to e.g. Brutsaert (1982), Stull (1988), Garratt and Pielke (1990) and Garratt (1992). There is now widespread, though not universal, acceptance of a value of the von Karman constant in the range 0.38 to 0.41.

Variances

For a discussion on the scaling of variances, and a summary of observations, the reader should consult e.g. Garratt (1992). For observations of σ_w and σ_T in unstable conditions, the stability dependence based on a number of field observations can be found in Kader and Yaglom (1990) — see Fig. 8. For observations over a wide range

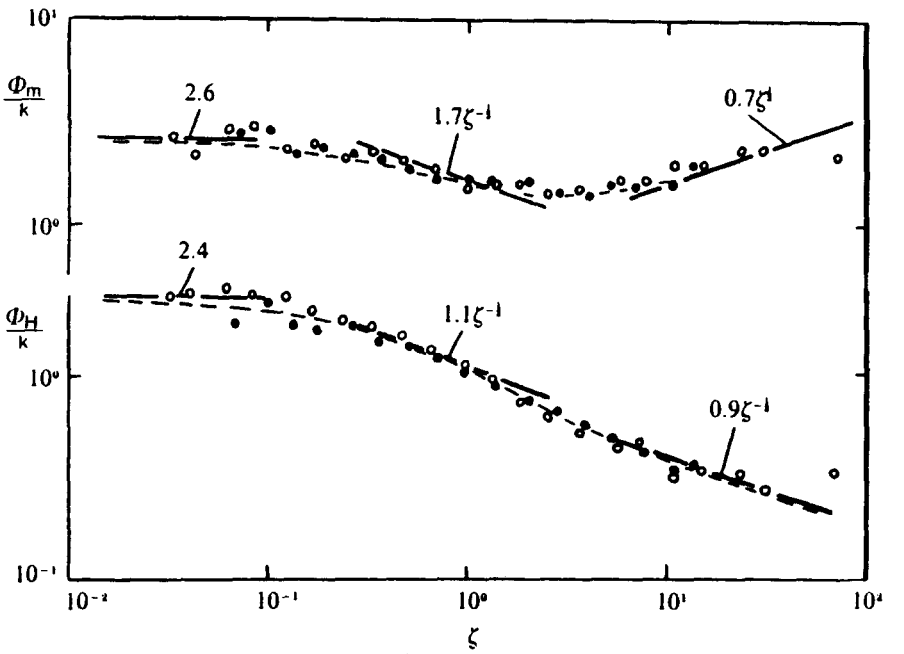

Fig. 7. Dimensionless velocity and temperature gradients (Φ_M/k and Φ_H/k) as a function of $\zeta = -z/L$ in unstable conditions based on observations, with specific functional forms shown — from Kader and Yaglom (1990).

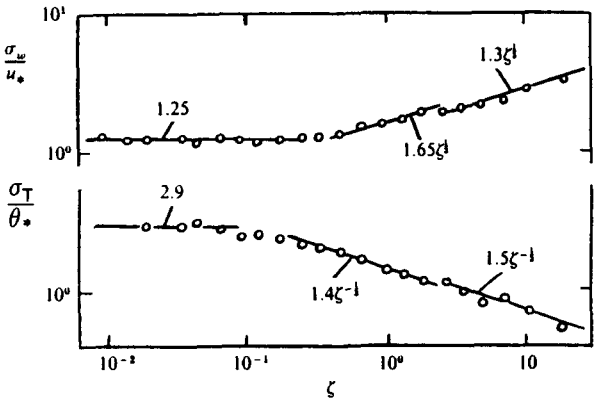

Fig. 8. As in Fig. 7, for σ_w / u_* and σ_T / Θ_*.

in z/Λ (here Λ is the equivalent of L, but defined in terms of local not surface fluxes) at low levels throughout the stable NBL, where Monin–Obukhov scaling breaks down and local scaling is appropriate (i.e. where local values of u_* and Θ_* are relevant), the reader should consult Sorbjan (1989; his figs. 4.20, 4.21).

Spectra and cospectra

The curves of Kaimal et al. (1972) based on observations made during the Kansas experiment (Izumi, 1971) are still the most comprehensive, covering both unstable and stable conditions.

4.2. ABL and mixed layer over land

Mean profiles

Validation of ABL similarity theory was provided in an analysis of Wangara observations by Yamada (1976), who determined normalised wind and temperature profiles in both unstable and stable conditions. His analysis provided the first substantial experimental evidence for the stability dependences of the A, B and C functions appearing in Eqs. (12)–(14). For further information on these functions, and the tendency for stability effects to be dominant, the reader should consult e.g. Brutsaert (1982) and Garratt (1992). Some estimates of these functions over non-homogeneous terrain have been provided based on analysis of observations from FIFE (e.g. see Sugita and

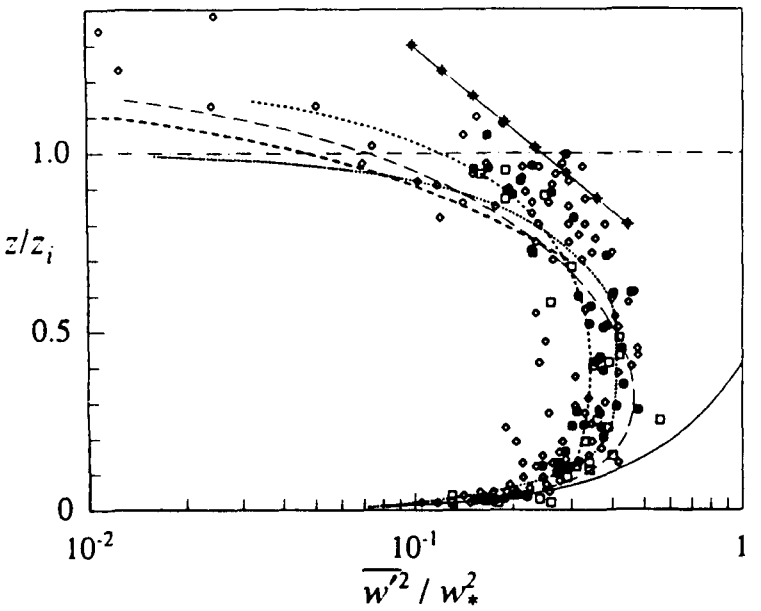

Fig. 9. Dimensionless profile of vertical velocity variance in convective conditions for a range of observational data and specific functional forms — over land and sea, and in the laboratory. See Hess (1992) for details.

Brutsaert, 1992). They are useful for estimation of regional surface fluxes.

Variances

Variances and higher-order moments have been measured throughout the ABL in both stable and unstable conditions, and modelled successfully using LES models in neutral conditions. Systematic behaviour of a range of turbulent statistics is evident if the appropriate scaling is used (e.g. see Hess, 1992). Thus, in unstable conditions, this is achieved using convective scaling; typical results can be found in e.g. Sorbjan (1989, figs. 4.32, 4.33) and Garratt (1992, p. 77) for profiles of σ_w (also u and v components) and σ_T. Composite sets of data for both land and sea have been discussed in Hess (1992) and profiles of σ_w and σ_T suitably nondimensionalised are shown in Figs. 9 and 10. Also shown are laboratory data which, in the lower half of the CBL, agree well with atmospheric observations. Differences aloft are probably related to the effects of clouds and vertical wind shear in the observations, both which affect entrainment dynamics.

In stable conditions, local scaling is required, and typical results appear in Caughey et al. (1979) and Nieuwstadt (1985) for the covariance (flux) profiles, and in Caughey et al. (1979) and Sorbjan, (1989, figs. 4.23, 4.24) for variances. For the neutral ABL, LES results for the covariance profiles can be found in Mason and Thomson (1987), as summarised in Garratt (1992, p. 48).

Spectra / cospectra

Suitably nondimensionalised, the observed spectra and cospectra described by Kaimal et al. (1976) (also see Sorbjan, 1989; p. 143) for the unstable mixed layer, and by Caughey et al. (1979) for the stable ABL (also see Garratt, 1992, p. 82) represent the most comprehensive set of curves to date.

5. Marine / cloudy ABL

In many situations, clouds exist within or immediately above the ABL over the ocean. Put another way, most observations of the cloud-topped boundary-layer (CTBL) have been obtained over the ocean where ABL clouds, particularly in the form of stratocumulus, are common and often persistent over many days at any given locality. Experimental studies have tended to focus on three boundary-layer types

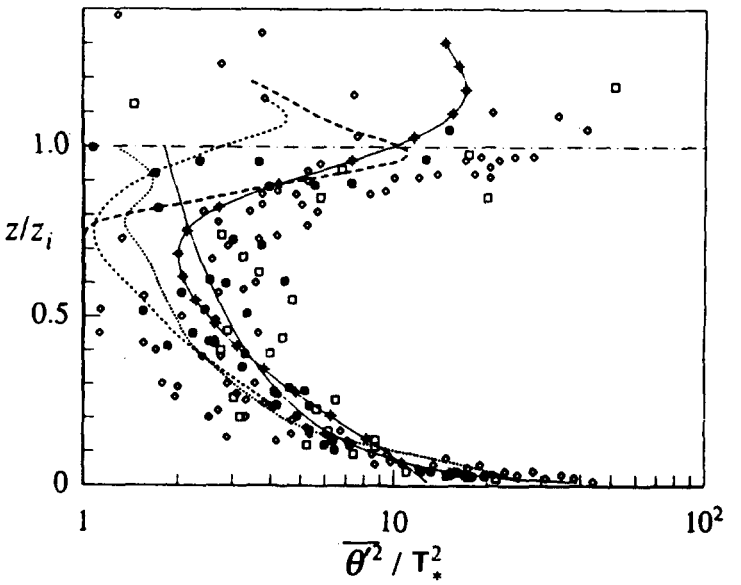

Fig. 10. As in Fig. 9, for dimensionless temperature variance. See Hess (1992) for details.

(i) The tropical and sub-tropical marine ABL, usually associated with cumulus (Cu) and stratocumulus (Sc) clouds.

(ii) The mid-latitude marine ABL (open ocean), associated with Cu and Sc clouds.

(iii) The sub-tropical and mid-latitude marine ABL generated during cold-air outbreaks to the east of the continental land masses, associated with Sc and Cu cloud formation.

The marine ABL during cold-air outbreaks can be highly unstable with latent heat fluxes well in excess of the sensible heat fluxes (e.g. Francey and Garratt, 1978; Chou, 1993). Absolute values of the evaporation rates can reach nearly 1000 W m^{-2} in extreme conditions.

Major boundary-layer cloud types are stratocumulus, stratus and fair-weather cumulus, and these serve as suitable foci for a discussion of the cloudy ABL.

5.1. Stratocumulus

Observations reveal the following broad categories of stratocumulus-topped ABL

(i) a fully mixed ABL, with a single elevated cloud layer fully coupled with the sub-cloud layer. This type of CTBL is usually associated with either significant surface heat fluxes or strong radiative cooling at cloud top;

(ii) a single cloud layer decoupled from the surface, in which mixing is the result of cloud-top radiative cooling. The cloud forms part of a detached turbulent layer, whose base is separated from the true ABL (i.e. the mixed layer adjacent to the surface). Surface fluxes are usually quite small;

(iii) a fully mixed single layer, or layer in which two or more separated turbulent layers exist, which supports multiple cloud layers (not necessarily all being stratocumulus). If more than one cloud layer exists, the intervening layer of clear air may serve as a barrier to vertical mixing.

Fully-coupled single layer

This layer may be predominantly surface driven due to heating or friction associated with strong winds, or it may be cloud-top driven due to strong radiative cooling. In the latter case, cloud-top radiative cooling may be intense enough, in situations where surface fluxes are small, to support a convectively mixed layer extending from the cloud top to the surface.

Examples of mean profiles of thermodynamic variables are shown in Fig. 11 for a thick stratocumulus layer. The ABL is fully mixed because of the combination of non-negligible surface fluxes in moderate to strong winds, and the existence of cloud-top radiative cooling. Through the cloud layer Θ or Θ_v increases according to moist adiabatic ascent, whilst Θ_e is approximately constant. Of particular significance are the large jumps in properties across the ABL top.

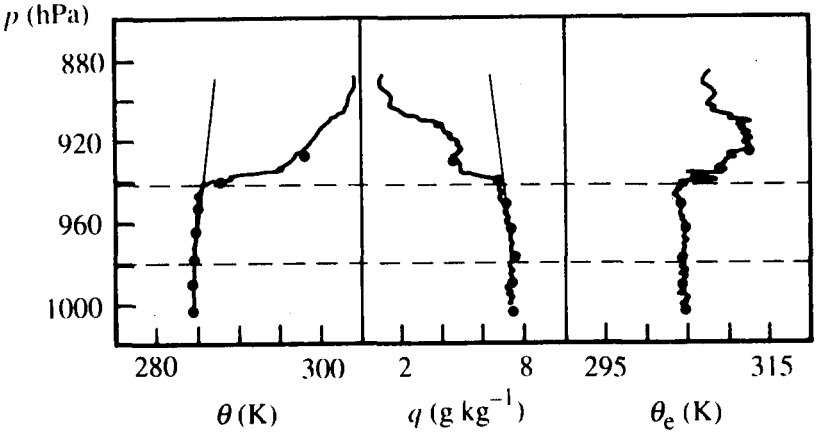

Fig. 11. Vertical profiles of several thermodynamic variables in the CTBL offshore from California in a situation of thick continuous stratocumulus cover (denoted by pecked lines). See Garratt (1992; fig. 7.3) for further details.

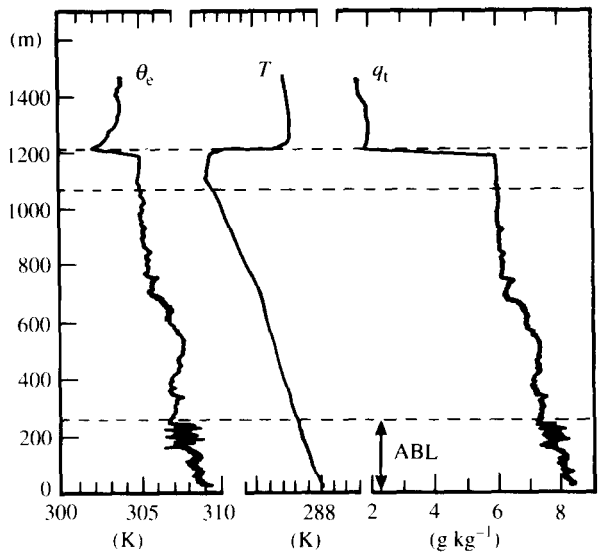

Fig. 12. Vertical profiles of several thermodynamic variables in the CTBL over the north-east Atlantic for a decoupled stratocumulus layer (top pair of pecked lines). Here, $q_t = q + q_l$. The bottom pecked curve corresponds to the top of the Ekman layer. See Garratt (1992; fig. 7.5).

Decoupled single layer

An example of a decoupled stratocumulus layer is shown in Fig. 12. The cloud layer is barely 150 m thick and located beneath a sharp inversion. The dry adiabatic lapse rate and fluctuations in the wind components indicate that turbulent mixing extends beneath cloud base and into the sub-cloud layer. This whole mixed region has essentially the same values of Θ_e and total humidity q_t, and is decoupled from the true ABL or surface-based Ekman layer (of height $\approx 0.2\, u_*/|f|$), in which turbulence is maintained to a height of about 280 m by surface-related processes, as a result of an intervening stably stratified layer.

Multiple layers

Though not shown in diagrammatic form here, a good example of multiple layers can be found in Nicholls (1985). In this case (from the JASIN experiment in the north-east Atlantic), coupling between a stratocumulus layer of thickness about 350 m and the surface-based ABL of depth 400 m was generally weak and intermittent, mainly because of small surface heat fluxes related to near-neutral stability conditions. The local condensation level coincided with the top of the shallow ABL and, in the presence of conditional instability above ($\partial\Theta_e/\partial z < 0$), a field of cumulus clouds extended into the overlying stratocumulus. Even though the cumulus was observed to be intermittent and irregularly distributed in the horizontal, it acts to transport mass (water vapour) from the ABL towards the stratocumulus layer.

5.2. Stratus

Observations of stratus cloud layers have tended to concentrate on the Arctic region in summertime, with very few comprehensive data from elsewhere. Nevertheless, observations to date seem to suggest at least two main categories of stratus-topped ABL

(i) a fully mixed ABL, with a single elevated cloud layer fully coupled with the sub-cloud layer. This type of CTBL is associated with moderate to strong winds and negligible buoyancy effects. The vertical velocity variance typically shows little enhancement near cloud top so that buoyancy effects are probably not significant (Nicholls and Leighton, 1986);

(ii) an ABL above which several low-level cloud layers exist.

5.3. Cumulus

Boundary-layer cumuli are cumulus clouds whose vertical extent is limited by the main subsidence or capping inversion. Such clouds are generally non-precipitating, and are usually referred to as fair-weather cumulus, cumulus humilus, or trade-wind cumulus. Boundary-layer cumuli are often composed of an ensemble of forced, active or passive clouds (Stull, 1985) with the deepest of these, the active clouds, ascending no more than a few km above the main inversion.

Forced cumulus clouds form within the top of mixed-layer thermals while the thermals are overshooting into the overlying stable layer. These thermals remain negatively buoyant during the overshoot, even though there is warming from condensation. Thus, the visible thermal rises

above the local condensation level, but fails to reach its level of free convection (where a parcel will have positive buoyancy relative to the environment). Active cumulus clouds ascend above the level of free convection and thus become positively buoyant. Because of this they tend to ascend to greater heights than forced clouds and develop circulations that are independent of the original triggering thermals. In the forced case, little or no transport (venting) of ABL air into the free troposphere occurs whilst, for the active case, transport does take place. Finally, passive clouds are the decaying remnants of formerly active clouds and, in general, have no interaction with the ABL, except that they shade the ground (as do other non-ABL clouds).

How is the turbulence structure and the vertical fluxes affected by the presence of cumulus clouds? It is apparent from both observations (usually involving aircraft) and modelling studies that, where clouds are present and particularly fair-weather cumulus, the moisture flux near cloud base is a significant fraction of the surface evaporation. In contrast, entrainment moisture fluxes near the mixed-layer top in clear skies are usually small. This is evident in the observations described by LeMone (1980) — see Fig. 13 — which also reveal small virtual heat fluxes at cloud base. These data, in fact, illustrate the slightly unstable conditions often found over tropical and sub-tropical open ocean areas, under fair-weather conditions, where h/L is typically in the range -10 to -1. The surface sensible heat flux and virtual heat flux are small, but evaporation rates relatively large; the radiative cooling near cloud base tends to maintain a sub-cloud

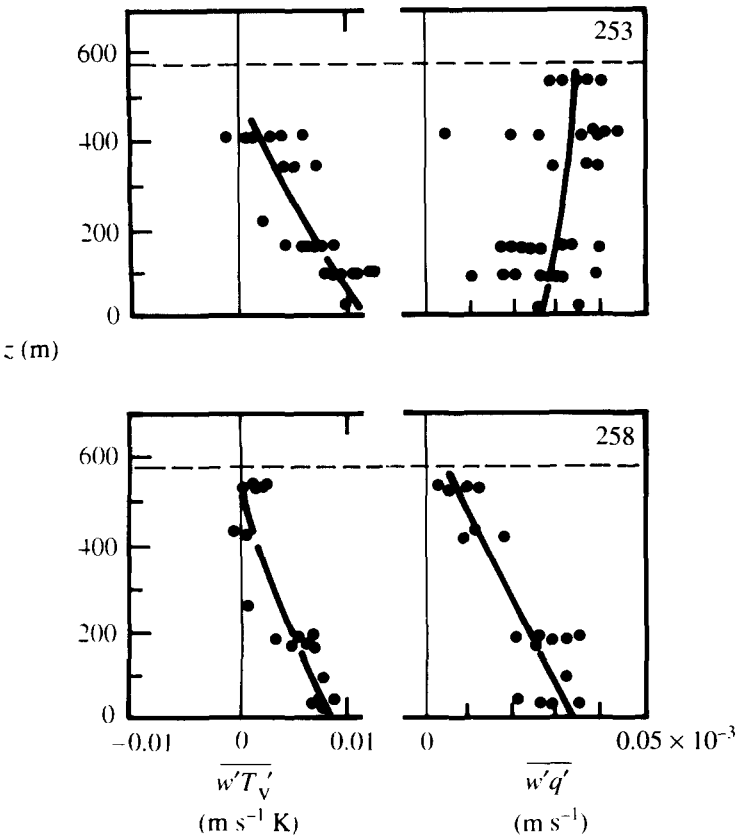

Fig. 13. Profiles of heat and moisture fluxes for two GATE days, the upper for a cloudy ABL and the lower for clear skies. Pecked curves show the approximate level of cloud base and/or ABL top — based on LeMone (1980).

layer cooler than the sea (Betts and Ridgway, 1989).

We can summarise important observational aspects of the stratus- and stratocumulus-topped ABL as follows

(i) As with the clear ABL, strong jumps in Θ_v and q occur across cloud top (defined as the ABL top), with Θ_e often showing both positive and negative jumps. The change in Θ_e across the cloud top is an important parameter characterising entrainment, and is closely associated with strong cloud-top radiative cooling and cloud-layer stability.

(ii) In the presence of strong winds, large surface fluxes or large entrainment effects (related to cloud-top radiative cooling), the CTBL is well mixed, with the cloud layer coupled to the sub-cloud layer and to the surface. The top of the ABL usually corresponds with cloud top.

(iii) In light to moderate winds, with negligible surface fluxes of sensible heat and momentum, the cloud layer is decoupled from the surface. In this case, the CTBL is not well mixed.

(iv) The CTBL may consist of more than one cloud layer.

(v) Precipitation in the form of drizzle may occur, with a tendency towards stabilization of the CTBL. The stability is affected because the cloud layer is associated with the latent heat of condensation, whilst in the sub-cloud layer evaporative cooling occurs.

(vi) In some instances, the cloudy stratiform ABL is convective in nature and has a number of similarities with the clear CBL heated from below. Generally though, the main source of buoyancy for this CTBL is at the entraining boundary and there are additional sources and sinks of TKE associated with radiative effects and phase changes. It is unlikely that any single method of scaling data obtained in convective layers containing stratocumulus will yield results which have universal applicability since the TKE balance is potentially much too complicated. At other times, particularly under strong wind conditions, the CTBL is indistinguishable in a dynamical sense from the neutral ABL without clouds.

6. Non-homogeneous abl over land

6.1. Introduction

Significant horizontal variations in ABL structure and properties usually arise from heterogeneity in surface properties, though they may also be induced by horizontal variations in cloudiness. Even at the microscale (order of tens of metres), surface variations can induce an organised response in the form of internal boundary layers, though these are usually confined to the lowest few metres or tens of metres. Indeed, for surfaces whose heterogeneities are disorganised at length scales somewhat less than 10 km, there is no apparent organised mesoscale response in the lower atmosphere. For surfaces that have organised heterogeneities at scales greater than 10 km, there may be an organised mesoscale response throughout the ABL and above. Fig. 14 illustrates this schematically. The response of area-averaged evaporation at these two scales to the imposed available energy, surface and atmospheric conditions may also be different (Shuttleworth, 1991).

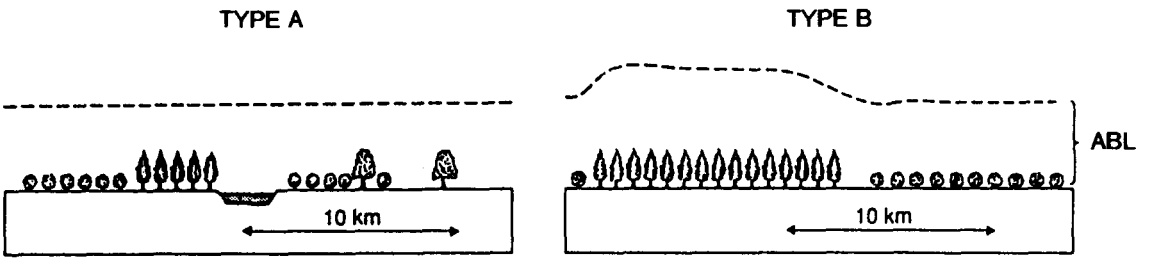

Fig. 14. Classification of land surface types (two) based on Shuttleworth (1991). In type A, the surface structure is disorganised at length scales of 10 km or less; in type B, there is organisation at length scales greater than 10 km.

The problem of surface heterogeneity can be considered on several scales. On the smallest scale, the response is confined to the surface layer and is dominated by local advection effects. The ABL as a whole can then be taken as horizontally homogeneous. At the next larger scale, the effects of the surface disturbance can be followed downwind until the whole of the ABL is affected. This is the case of mesoscale advection. Finally, at this scale and larger, the ABL adjusts to the new surface conditions and, under optimum large-scale conditions, mesoscale circulations develop (sea breezes, lake breezes, inland breezes) which interact further with the horizontally varying ABL. Surface heterogeneity can also be identified with changes in surface elevation, as occurs in regions of hills, ridges and valleys. Under these conditions, large scale changes in the pressure field are induced producing a complex response in the ABL flow.

6.2. Major field experiments

HAPEX-Mobilhy took place in south-west France for 3 months in 1986 under the framework of the World Climate Research Programme (WCRP) of WMO. The focus was on a program of observations and modelling aimed at studying the water budget and evaporation at the scale of a GCM grid. One main objective was to provide a data base against which parametrisation schemes for the land surface water budget can be tested and developed. Several aspects of the experiment and results have been reported, including an overview (Andre et al., 1986), initial results (Andre et al., 1988); regional estimates of fluxes and comparisons of aircraft fluxes with surface measurements (Andre et al., 1990); application of a mesoscale model using an advanced surface parametrisation (Bougeault et al., 1991a, b; Noilhan et al., 1991); canopy processes and applications (Mehrez et al., 1992a; Pinty et al., 1992); calibration of a bare soil energy model (Mehrez et al., 1992b). In addition, the complete data set is readily available from the French group (see e.g. Andre et al., 1990).

There is no doubt that the HAPEX-Mobilhy experiment has resulted in a high quality comprehensive data set focussing on aspects of ABL structure on selected days, and surface energy

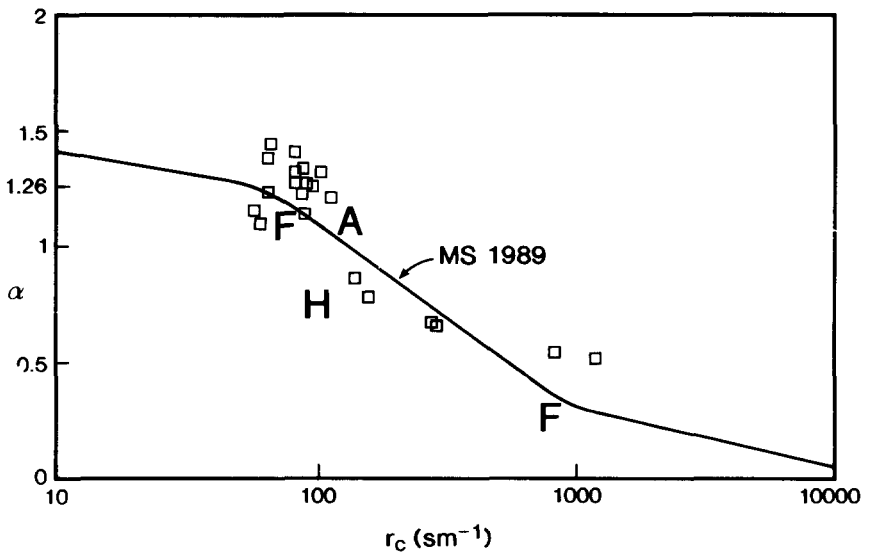

Fig. 15. Dependence of the Priestley–Taylor coefficient α upon canopy stomatal resistance r_c; a value of 1.26 is the accepted value for homogeneous saturated surfaces. Of particular interest is the mean values for the FIFE (F) and ARME (A) experiments — both type A surfaces — and for the HAPEX (H) experiment — a type B surface. Other observational data, and the curve, are from McNaughton and Spriggs (1989). After Shuttleworth (1991).

and water budgets at several locations over a period of 3 months. The data have proved invaluable for validation and calibration of new surface and ABL schemes used in mesoscale and climate models.

FIFE — the first ISLSCP field experiment (see e.g. Sellers et al., 1988) took place in east Kansas in 1987 and 1989, with major observing periods focussed within a 15×15 km region of Konza prairie. One of its major objectives concerned the use of satellite observations to infer climatologically significant land-surface parameters.

The first set of major results has been described recently in a special issue of *Journal of Geophysical Research* (Vol. 97, No. D17, 1992). Studies have focussed on six areas, as follows: (i) ABL, with particular emphasis on airborne fluxes and measurement techniques; (ii) Surface Fluxes, with emphasis on heat, moisture and CO_2 fluxes and sensor performance; (iii) Correction and calibration of satellite sensor data; (iv) Surface radiation and biology; (v) Soil moisture; (vi) Integrative science. The results to date have led to improved understanding of the exchanges between the land surface and atmosphere at the local scale (1–100 m) and at the intermediate scale (100 m to 15 km). In addition, much is being learnt on the application of remote sensing science at these two scales, and the use of remote sensing and modelling at the intermediate scale. The application of FIFE data to validation of model simulations has recently received some attention, with emphasis on aspects of surface and boundary-layer behaviour (Betts et al., 1993).

Both HAPEX and FIFE observations of evaporation have been used by Shuttleworth (1991) to illustrate the impact of land heterogeneity upon regional evaporation, and its relation with available (net radiant) energy and bulk canopy resistance (r_c). Fig. 15 shows the dependence of the Priestley–Taylor parameter α upon r_c, based on observations and predictions of a simple 1D ABL model with a range of initial conditions (note that α is directly proportional to $\lambda E/(R_N - G)$; the reader is referred to Priestley and Taylor, 1972). It is thought that the HAPEX anomaly reflects the impact of larger-scale heterogeneities, with significant mesoscale advection and circulations reducing the regional evaporation relative to the net available energy. This has important implications for the parametrisation of regional energy fluxes.

6.3. Internal boundary layers

General

Internal boundary layers (IBL's) in the atmosphere are associated with the horizontal advection of air across a discontinuity in some property of the surface. Studies usually specify the surface forcing in terms of a step change in surface roughness, temperature or humidity, or in the surface flux of heat or moisture. Several classes of IBL problem can be readily identified in the literature, concerning both laboratory and atmospheric flows, and related both to the thermal stability characteristics and horizontal scale of the flow.

Earlier work (from the late fifties to the mid-seventies) was concerned mainly with the problem of neutral flow across a step change in surface roughness. Later in this period, attention turned to the effects of thermal stratification upon the flow across a roughness change, and to the growth and structure of the IBL related to step changes in surface heat flux and temperature. Throughout this period the main emphasis was on the small-scale aspects of the flow i.e. on relatively small downwind fetches and where, in the atmosphere for example, the IBL was confined to the atmospheric surface layer of the advected planetary boundary layer. Such a constraint allowed for several simplifying assumptions in analytical and numerical treatments, and confined the downstream fetch to maximum values of about 1 km.

In more recent times (the mid-seventies to the present), the emphasis moved from the micrometeorological (and local advection) problem associated with relatively small fetches to mesoscale advection, and in particular to the effects of buoyancy and the development of the thermal IBL towards an equilibrium boundary layer far downstream of the leading edge (relatively large fetches). The main topic has been on the growth

of the convective thermal internal boundary layer (TIBL) at the coast, mainly because of practical concern on the influence of the IBL on coastal pollution from industrial sites located in the coastal region. Less attention has been given to the parallel problem of a stably stratified IBL, whose full development may require fetches of several hundreds of km. For a recent review of the topic, and many relevant references, see Garratt (1990). We limit the present discussion to the problem of mesoscale flow and IBL growth as schematically shown in Fig. 16.

Most mesoscale studies focus on the structure and growth of the TIBL, and stem from the perceived relevance of the IBL to diffusion and pollution problems in the coastal region. Although the advection of air across the coastline relates to both surface roughness and temperature changes, the primary consideration is often the response and growth of an IBL to a marked step-change in surface temperature. It is recognised that in real world situations roughness changes also are present. The emphasis generally has been on the growth equation for the IBL depth in both convective and stable conditions, and the factors affecting the depth. Definition of the thermal IBL is usually in terms of the marked changes in temperature and humidity gradient found near its top, and this seems to be most appropriate for the stable case. Observations of

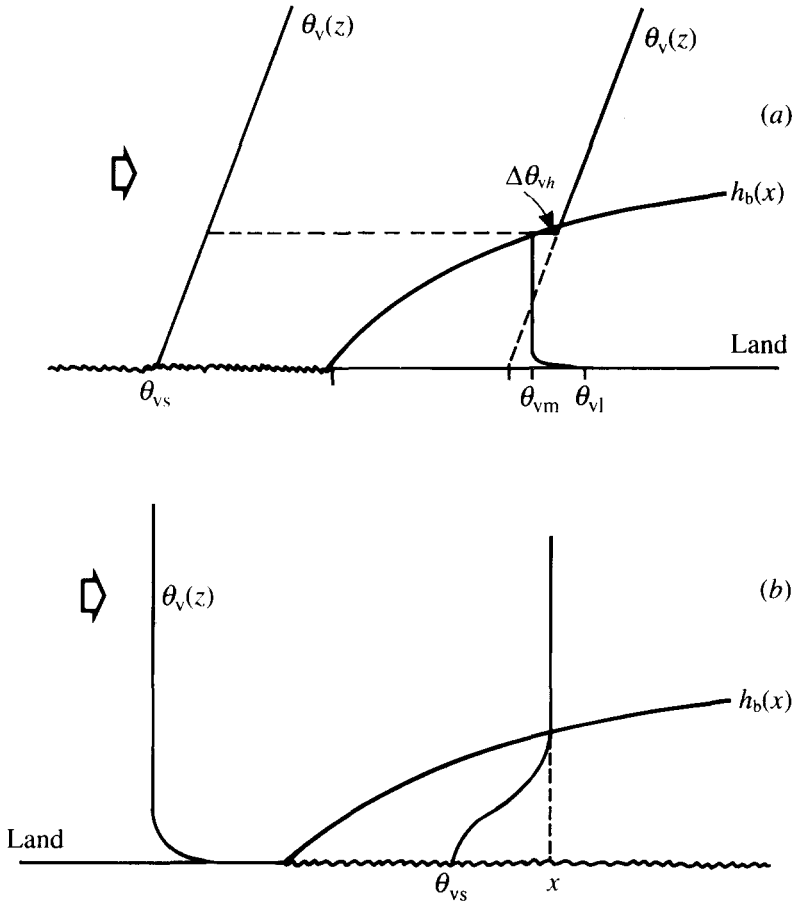

Fig. 16. (a) Schematic Θ_v profiles under conditions of onshore flow and formation of a convective IBL of depth $h_b(x)$; (b) As in (a) but for offshore flow and formation of a stable IBL.

convective TIBL structure (usually for fetches less than about 50 km) during sea-breeze events and for general onshore flow conditions have found that the top defined from the Θ profiles can be well below the level of minimum turbulent kinetic energy. Such observations of the mean and turbulence structure reveal the IBL as a fairly well-mixed layer, with large horizontal gradients in Θ_v and turbulent kinetic energy for several tens of km inland from the coast. In contrast, turbulence closure-model studies of the TIBL structure and growth (e.g. Durand et al., 1989) reveal that the TIBL top defined in terms of the Θ_v inversion layer tends to coincide with the level of near-zero heat flux and turbulent kinetic energy, and with maximum temperature variance.

The convective thermal IBL

The convective IBL (depth h_b) usually forms over land under clear skies during the daytime when there is an onshore flow of air. Simple models of convective IBL growth can be developed from a slab-model approach, based on mixed-layer dynamics. This can be used to derive a set of governing equations from which $h_b(x)$ can be determined, where the fetch is designated as distance x from the coastline (Fig. 16a). Equations for mixed-layer wind components and temperature, the continuity equation and an equation for h_b permit numerical solution, with appropriate boundary conditions. The h_b equation required for closure results from applying the TKE equation (Eq. 6) at the inversion level and utilising a suitable entrainment assumption.

For practical application, it is possible to derive a suitable model, based on the steady state, pure advective case, with equations identical to those for the growing CBL over a homogeneous surface. The reader is referred to Garratt (1990) for details. If we assume that the lapse rate γ_θ is constant and that the surface heat flux is independent of x, and use the initial condition that $h_b = 0$ at $x = 0$, then, with u_m the slab velocity, we have

$$h_b^2 = 2(1 + 2\beta)(\overline{w'\theta_v'})_o x/\gamma_\theta u_m \qquad (29a)$$

so revealing an $h_b \propto x^{1/2}$ behaviour (e.g. Venkatram, 1977). For practical application, the heat flux may be parametrised in terms of a bulk relation using suitable transfer relations.

Most observational studies have been confined to inland fetches in the range 5 to 50 km, since this is the typical distance required to approach the full depth of the ABL. Growth of the TIBL over this fetch range has generally supported the relation $h_b = ax^{1/2}$, with h_b and x both in metres, and with a in the range 2 to 5 approximately. These numerical values can readily be shown to be consistent with that implied in Eq. (29a). If we take $\beta = 0.2$, and $\gamma_\theta = 0.01$ K m^{-1} (a rather large value), then

$$h_b^2 \approx (2.8/0.01)(\overline{w'\theta_v'})_o x/u_m. \qquad (29b)$$

Realistic values of $u_m = 5$ m s^{-1} and $H_o = 100$ W m^{-2} give $a \approx 2$, whilst $u_m = 2$ m s^{-1} and $H_o = 400$ W m^{-2} give $a \approx 7$. Decreasing γ_θ to a low value of 0.001 K m^{-1} increases these a values by a factor $10^{1/2}$. Thus, a values lying in the range 2 to 22 can be expected and are comparable with observed values (Hsu, 1986).

This $x^{1/2}$ behaviour is found because stationarity is assumed as well as horizontal uniformity of the heat flux. The effect of a time varying heat flux can be readily deduced if the heat flux is assumed to vary sinusoidally through the day (a good approximation). Let $H_o = H_o^{max} \sin(2\pi t'/T)$, where $T = 24$ hours and t' is the time elapsed since sunrise and also the time at which air crosses the coastline. If t is the travel time from the coast to a point x inland, the TIBL height at time t can be found from (Garratt, 1992; p. 188)

$$\begin{aligned} h_b^2 &= 2\gamma_\theta^{-1}(1 + 2\beta)\int_{t'}^{t+t'} (H_o^{max}/\rho c_p) \\ &\quad \times \sin(2\pi t''/T)\, dt'' \\ &\approx 2\gamma_\theta^{-1}(1 + 2\beta)(H_o^{max}/\rho c_p)(T/2\pi) \\ &\quad \times \{\cos(2\pi t'/T) - \cos[2\pi(t + t')/T]\}. \end{aligned} \qquad (30)$$

The depth of the TIBL after a travel time t ($= x/u_m$) depends on t' since this sets the average level of the heat flux during the passage of the air to a point x inland from the coastline. For

$t' = 0$, the air crosses the coast at sunrise when the heat flux is zero over the land surface whilst if $t' = T/4$ the air crosses at midday when the heat flux is maximum. Growth of the TIBL will be greater near midday than near sunrise. What typical travel times are appropriate? For the TIBL depth to approach the "equilibrium" CBL depth expected "far inland", t of order 1 hour suffices, noting that for $t' = 0$, the CBL will be shallow (≈ 100 m) and for $t' = T/4$, the CBL will be approaching its maximum daytime depth (≈ 1–2 km). Two solutions of Eq. (30) serve to illustrate the problem,

(i) With $t' = 0$ and $t = x/u_m$ ($\ll T$),

$$h_b^2 = 2\gamma_\theta^{-1}(1 + 2\beta)\left(H_o^{max}/\rho c_p u_m\right)\left(2\pi x^2/u_m T\right) \quad (31a)$$

(ii) With $t' = T/4$,

$$h_b^2 = 2\gamma_\theta^{-1}(1 + 2\beta)\left(H_o^{max}/\rho c_p u_m\right)x. \quad (31b)$$

Thus, after one hour's travel time inland from the coast ($x/u_m = 1$ hour) the midday IBL will be greater than the early morning IBL by a factor $(u_m T/2\pi x)^{1/2} \approx 2$. The analysis also shows that the stationarity assumption is likely to be much better around the time of maximum heat flux when, for an assumed sinusoidal variation, the heat flux undergoes its minimum rate of change with time.

At very large fetches, boundary-layer heights must tend towards an equilibrium value. That is, the square root dependence must ultimately be invalid at large enough x where h_b tends to a constant value. In addition, the lapse rate γ_θ is likely to vary with x, particularly at fetches where the IBL top approaches the level of the subsidence inversion. In the context of Eq. (29a), whose differential with respect to x constitutes an IBL growth equation, a large increase in γ_θ at the inversion will reduce the rate of growth of the IBL considerably.

The stable thermal IBL

Much of the interest in the stable case is related to offshore flow in the coastal region from warm land to cool sea. Growth of the stable thermal IBL has mostly been studied by appeal to historical data and dimensional analysis (Mulhearn, 1981; Hsu, 1983), by use of numerical and simple physical models (Garratt, 1987), and by analysis of detailed aircraft data (Garratt and Ryan, 1989). Growth rates are found to be small, with fetches of several hundreds of km required to develop an IBL several hundred metres deep. The nature of the Θ_v profiles within the IBL over the sea is found to be quite different to that found in the stable boundary layer over land. Over the sea, the Θ_v profiles are found to have large positive curvature with vertical gradients increasing with height, interpreted as reflecting the dominance of turbulent cooling within the layer. The behaviour contrasts with the behaviour in the nocturnal boundary layer over the land, where curvature is negative (vertical gradients decreasing with height) and where radiative cooling is dominant (Garratt, 1990).

A suitable model of IBL growth can be formulated based on the basic structure shown in Fig. 16b. We assume for simplicity that the advected continental mixed-layer air of virtual potential temperature Θ_{vc} remains constant. Above the IBL we take $\gamma_\theta = 0$. The starting point is the 2D, steady-state Θ_v equation (Eq. 3) integrated between the surface and h_b, with an assumed linear flux profile and assumed self-preserving forms for the profiles. The result for $h_b(x)$ is (Garratt, 1990)

$$h_b^2 = \alpha_1 U^2 \left(g\Delta\theta/\theta_v\right)^{-1} x \quad (32)$$

where

$$\alpha_1 = 2A_o f(z/h_b)\overline{Rf}C_g$$

and, U is a large-scale, or geostrophic, wind at a small angle to the IBL mean wind direction along which the x-axis is defined (thus, x is the actual fetch); $\Delta\Theta$ is the temperature difference between the IBL top and the surface; C_g is a boundary-layer heat transfer coefficient; $\overline{Rf}$ is a critical layer-averaged flux Richardson number and A_o is a positive profile shape factor with a value O(1).

The $x^{1/2}$ prediction in Eq. (32) and the dependence on other parameters, is generally confirmed by observations and numerical simulations, for $\alpha_1^{1/2}$ in the range 0.014 to 0.024 (Gar-

ratt, 1990). It is readily apparent that growth rates implied in Eq. (32) for the stable IBL are much less than those implied in Eq. (29) for the unstable IBL.

6.4. Flow over orography

Theory and other considerations

Sloping terrain. In the presence of uniform sloping terrain many aspects of ABL structure remain unchanged from that over horizontal surfaces. At nighttime, however, the presence of slopes can affect significantly the depth of the nocturnal boundary layer (NBL) and induce shallow drainage or katabatic flows almost independent of the overlying NBL. By day, upslope flows tend to be deep and the CBL little affected by the underlying slope.

The presence of sloping terrain is represented in Eqs. (1) and (2) by an additional buoyancy term; thus, with the x-axis taken along and down the slope, the RHS of Eq. (1) contains a new term, of the form $-(g/\theta)\Theta'\sin\alpha$ where the temperature deviation Θ', which is negative in stable conditions, produces a height dependent local pressure gradient. The slope of the terrain is represented by the angle α.

In the presence of sloping terrain, and hence of slope flows and interfacial mixing, NBL characteristics are modified compared with flow over a horizontal surface. Both numerical models and observational studies have been used to study the effects of slope. For example, Brost and Wyngaard (1978) used a simplified second-order ABL model to show how slope inclination and the relative direction of the large-scale wind affected NBL depth and internal structure. Garratt (1982) summarized observations and model results of the nondimensional NBL depth for a range of slope angles. Table 1 summarises these results and shows how the non-dimensional height parameter is sensitive to both the slope magnitude and the angle between the wind direction and the slope fall vector. The impact of katabatic flow in the Koorin case is clearly evident, with the reduced value of γ_e (see Eq. 28) being the result of a significant slope angle and a cross-slope geostrophic flow.

Table 1
Observed values of the Zilitinkevich constant γ_e (Eq. 28) for 4 sites, together with numerical values based on 1D NBL simulations, illustrating the effects of slope (magnitude α). Model calculations incorporate the observed wind direction relative to the sloping terrain, with appropriate values of latitude (ϕ) and roughness length (z_o). Data from Garratt (1982)

Site	ϕ	z_o (m)	α	γ_e	
				Observed	Calculated
Koorin	−15	0.1	0.002	0.13	0.14
Minnesota	45	0.01	0.001	0.37	0.38
Wangara	−30	0.001	0	0.39	0.37
Cabauw	45	0.1	0	0.42	0.39

Flow over hills. The study of flow over ridges and hills represents an extra degree of complexity compared with flow over horizontal or sloping terrain, or even flow across a simple change in surface conditions. The pattern of flow around a hill is determined not only by the hill shape but also by its size. If the hill is large enough (usually of height > 100–500 m) and occupies a significant fraction of the daytime ABL depth then flow disturbances throughout the ABL and into the stable region above will result (both day and night). For smaller hills, flow disturbances within and above the NBL only can be expected.

To a greater degree than in many other areas, our understanding of hill flow has been shaped by mathematical modelling. This is not surprising when instrumentation used in 1D micrometerological experiments must be located in a multitude of locations to capture the complex (3D) flow field around even simple topography (see the review by Taylor et al., 1987). At Askervein Hill, the site of the most complete field experiment to date, 50 towers were deployed with 27 of them equipped with three-component turbulence sensors (Taylor and Tuenissen, 1987). The most influential theoretical work to emerge has relied upon techniques of asymptotic matching applied to flow over low hills, where the equations of motion (Eqs. 1, 2) can be linearized (Jackson and Hunt, 1975; Hunt et al., 1988a, b). There is a great deal more structure to be explored in the

mean flow above an arbitrary hill than in the horizontally homogeneous and advective situations discussed above. In the lowest layer, the inner layer, whose thickness depends on the size and roughness of the hill, the Monin–Obukhov similarity theory can be used in modified form, but farther from the surface the presence of advection does not allow the condition of local equilibrium in the turbulence that such scaling requires (see Kaimal and Finnigan, 1993; ch. 5).

Field experiments and observational studies in complex terrain

We summarise below several relevant experiments and results of observational analyses that provide some insight into ABL structure and behaviour over regions of complex terrain.

(i) SESAME (1979) — this included, inter alia, studies of the low-level jet over the Great Plains of the USA (e.g. Lenschow et al., 1988a, b).

(ii) ALPEX (1982) — the emphasis, inter alia, was on ABL aspects of flow around and within the European Alps (e.g. see Smith, 1986 for research in the US; see volume 36, pp. 1–296 of Meteorol. Atmos. Phys., 1987). The main ALPEX experiment was held during March and April in 1982.

Studies related to the ABL were mainly concerned with diurnal heating effects, particularly on valley and slope winds, and on the local wind systems themselves. For example, Hafner et al. (1987) studied the diurnal variation in ABL structure on both sides of the Alps in the context of the regularly observed elevated heat low. Vergeiner and Dreiseitl (1987) summarised valley-wind research, emphasising the importance of quasiperiodic thermal forcing in driving local wind circulations, and the role of slope winds and topographical relief. They found that the diurnal variation in the horizontal thermal contrast between plains and valley induces a like pressure gradient variation, thus forcing both up- and down-valley winds. Finally, Hennemuth (1987) discussed the role of small valleys in the interplay of thermal circulation systems, and how these related to heating of the mountain ABL.

ABL observations from ALPEX in the Pre-Alps region of Switzerland have been analysed and described by Kustas and Brutsaert (1986) and Brutsaert and Kustas (1985, 1987). The Pre-Alps region is characterised by hills of the order of 100 m above the valley elevations and by distances between ridges of the order of 1 km. The emphasis in the first study was on the near-neutral wind profile and the relation between z_0, the zero-plane displacement and the surface geometry. This profile was found to be logarithmic over a substantial part of the ABL depth, leading to consistent results in estimating z_0 (about 3.5 m), d (about 45 m) and the friction velocity. In the second study, neutral humidity profiles were analysed, yielding values of z_q some 10 to 15 times smaller than z_0. In the third study, surface fluxes in unstable conditions were evaluated from measured vertical profiles using surface-layer relations (Eq. 8, for wind and humidity) applied throughout the lower half of the ABL. However, best results were found with the z/L dependence ignored and the Ψ functions replaced by a non-zero constant.

(iii) ASCOT (1984) — the overall objective of this major US dispersion-focussed experiment seemed to be a better understanding of pollutant transport and diffusion associated with valley flows, with particular emphasis on the transport of pollutants from energy related facilities to population or agricultural centres set within valleys. The original programme was developed in 1978, with major studies held in 1979, 1980 and 1981 in the Geysers geothermal area in northern California, USA (Gudiksen and Dickerson, 1983) and in 1984 in the Brush Creek valley in western Colorado, USA (see *Journal of Applied Meteorology*, Vol. 28, 1989).

(iv) MESOGERS (1984) — this ABL experiment involved studies of flow properties over inhomogeneous terrain and regional-scale fluxes (e.g. Durand et al., 1987; Weill et al., 1988).

(v) AUTAN (1984) — this ABL experiment studied the orographic influence on large-scale flow and its consequences on the dynamics of the local ABL (e.g. see Benech et al., 1987).

(vi) FIFE (1987, 1989) — see above. The essential requirements for FIFE were the need for simultaneous data acquisition and multiscale observations and modelling. Main ABL data con-

sisted of measurements of surface and near-surface fluxes from ground-based and aircraft systems, and of thermal and biophysical properties of the vegetation, and soil moisture. A strategy for optimum station distribution within the experimental area, and a discussion of estimating regional-scale surface fluxes from local values, can be found in Mahrt (1987).

(vii) HAPEX (1986) — see earlier discussion.

Theoretical / numerical studies in complex terrain

A number of these in the past few years have given new insight into ABL evolution over sloping or mountainous terrain, into ABL structure and terrain-induced mesoscale motions, and into the evolution of thermally-induced valley circulations.

For example, Banta (1984, 1986) was concerned with evolution of the daytime ABL over the Rockies, McNider and Pielke (1984) with general slope and mountain flows, and Segal et al. (1988) with the effects of vegetation on upslope flows. The ALPEX and ASCOT experiments have stimulated many theoretical and numerical studies related to ABL behaviour on the mesoscale — for example the work of Egger (1987a, b) and papers in the 1989 *Journal of Applied Meteorology* (Vol. 28) related to ASCOT. Egger's work involved the modelling of thermally-induced valley-plain circulations, with emphasis on clarifying the dependence of these upon the valley's geometry; stratification; advective processes and the diurnal cycle of heating. Model simulations which were highly resolving in the horizontal were able to produce the gross features of observed flows near the mouths of valleys.

Of particular relevance are the numerical studies of Han et al. (1982) and Deardorff et al. (1984) on the heated mixed layer over a mesoscale region of complex terrain. In part, they were interested in the problem of topographically-induced form drag, and evaluation of the related drag coefficients, over irregular terrain in the presence of a well-defined mixed layer. Their results are highly relevant to the problems of effective roughness lengths or drag coefficients for use in GCM's, and of sub-grid variability and how this should be represented in models. They found that during daytime the thermal effects of surface heating and entrainment on form drag were more significant than dynamic effects in an adiabatic, non-entraining ABL. Typical form-drag coefficients, for the example chosen of intermediate terrain variations, reached 0.005 in the middle of the day, greater than the frictional coefficient relative to a reference height of about 100 m. The work suggests how form drag might be parametrised in GCM's, a problem under fairly intensive study at present. These authors certainly question the use of effective roughness lengths in the standard ABL formulations, since they do not reflect the influence of ABL height and mixed-layer temperature variations at the mesoscale.

Nevertheless, much work has been reported on the problem of effective roughness lengths. For a mixed-cover landscape, the vertical flux of momentum to the surface is proportional to $[\ln(l_b/z_{oe})]^{-2}$, where z_{oe} is the effective roughness length and l_b is a blending height above which the effects of local IBL's are not felt. The following summary is taken from Hess (1992).

The effective roughness length for momentum can be estimated from a weighted average relation

$$\left[1/\ln^2(l_b/z_{oe})\right] = \Sigma_i\left[f_i/\ln^2(l_b/z_{oi})\right] \qquad (33)$$

where f_i is the fractional cover of local roughness length z_{oi}. Consideration of Eq. (33) for typical values of l_b in the range 10–100 m shows that the areal roughness length, and hence stress, is dominated by the roughest sub-areas and tallest roughness elements. Where orographic influences are present, terrain can play a significant role in determining surface roughness. Recently, Wood and Mason (1993) — see also the earlier study by Grant and Mason (1990) — parametrised the total drag by a sum of the shear-stress contributions associated with the small-scale roughness elements and form drag created by the terrain:

$$\ln^{-2}(z_m/z_{oe}) = C_a/k^2 + \ln^{-2}(z_m/z_{oi}) \qquad (34)$$

where C_a is a form-drag coefficient and z_m is a scale height approximately equal to the height of the obstacles (trough to peak for a ridge-valley system). A comparison of the predictions from

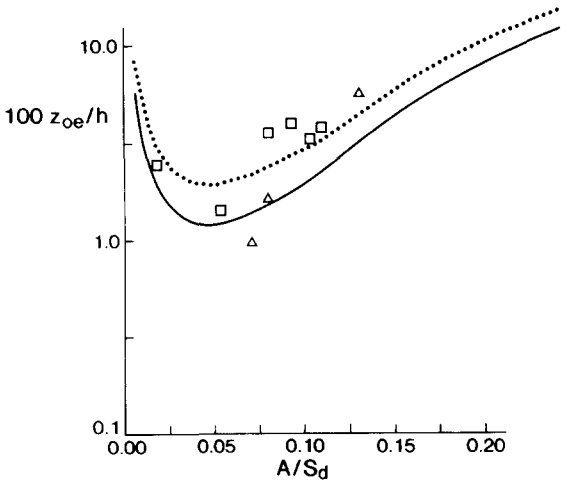

Fig. 17. The variation of z_{oe}/h (h here is the terrain height) as a function of a parameter A/S_d closely related to hill slope (here, A is the frontal or silhouette area of the hill, S_d is a base area). The squares are observed values from Grant and Mason (1990), triangles from Hopwood (1991). The solid line shows the prediction of Eq. (34) for two-dimensional hills with $z_o = 0.3$ m, $\lambda = 1000$ m; the dashed line is for hills with $z_o = 0.5$ m and $\lambda = 1000$ m. From Wood and Mason (1993).

Eqs. (33) and (34) with observations (Fig. 17) shows general agreement. Note that values of z_{oe} of several metres are implied under some circumstances, and that the ALPEX derived z_o of 3.5 m (second part of Section 6.3), with the terrain height $h = 100$ m and a terrain horizontal wavelength $\lambda = 1$ km, is entirely consistent with the results of Fig. 17.

6.5. Mesoscale circulations

Sea breezes

The diurnal cycle of onshore winds during the day and offshore winds at night is a characteristic weather feature in many coastal regions when synoptic-scale winds are light. This wind regime is generally referred to as the sea- and land-breeze circulation (Mak and Walsh, 1976).

Much has been learnt in the past three decades of the behaviour of sea breezes, and the ABL structure pertaining to the sea and land components of the complete sea-breeze circulation. In that time considerable research has been devoted to theoretical and observational aspects, and to numerical modelling. The sea breeze is basically a boundary-layer phenomenon and is a response to thermal forcing; it is driven by the differential surface heating between land and sea that occurs during the daytime. This induces a sea–land temperature difference of several Kelvins throughout the ABL, with the corresponding horizontal pressure gradient producing the sea-breeze circulation. Its intensity, longevity and inland penetration is significantly dependent upon several major factors including, dryness of the land surface, large-scale flow, terrain slope, latitude, insolation over land (e.g. Pielke, 1984 (ch. 13) and Arritt, 1989 for general overviews; Physick, 1980; Kondo, 1990; Bechtold et al., 1991; Arritt, 1993; for specific studies).

A recent review by Abbs and Physick (1992) discusses several aspects of sea breezes, including fine-scale structure, behaviour in complex terrain, inland penetration, role in internal-bore generation and numerical modelling. We summarise these issues here.

The sea-breeze front over land has strong similarities with a density current structure, the dense sea air that flows towards the front at low levels being swept up and backwards at the leading edge in the region referred to as the "head" (Simpson 1969, 1972). Mixing between cool moist sea air and warm dry land air takes place at the rear of the head through breaking billows (see Nakane and Sasano, 1986 for observations of these), generated at the front of the head by Kelvin–Helmholz shear instability. The mixed air flows back towards the coastline above the inflow and constitutes the return flow. A number of studies are relevant to the relation between the depths of the boundary layer, the inflow and the raised head (see e.g. Simpson and Britter, 1979). Typically, the inflow of depth several hundred metres flows into a mixed layer ahead of the sea breeze of depth 1 to 2 km, with the head about 2 to 3 times the depth of the inflow and extending back several kilometres only behind the leading edge (see e.g. Simpson et al., 1977; Nakane and Sasano, 1986; Kraus et al., 1990). Along the front during the day, the leading edge consists of a continually changing pattern of lobes and clefts about 1 km across. These arise from convective

instability caused by the overrunning of warm land air at the ground by denser sea air (Britter and Simpson, 1978), and disappear at night when radiative effects lead to cooling of the near-surface air. The first fine-resolution modelling study of the sea breeze to appear in the literature was published by Sha et al. (1991). They were able to simulate all the fine-scale features found in laboratory experiments and verify the empirical relations involving the inflow and head depths, and billow amplitudes and wavelengths.

The topography of the coastline has an important controlling effect on the sea breeze. As well as influencing the inland penetration it affects convergence/divergence and consequently the sea-breeze intensity and associated weather (see Abbs, 1986; Abbs and Physick, 1992). Coastal orography may also act as a barrier to the inland penetration of the sea breeze (Abbs and Physick, 1992). There is much evidence, both from observations and numerical experiments, that sea breezes do indeed travel large distances inland from the coast, the size of the penetration depending upon several factors including time of year (hence surface heating and moisture content) and latitude. Sea breezes have been observed as far as 280 km inland (Garratt and Physick, 1985), with many studies reporting penetrations of about 200 km (see references in Abbs and Physick, 1992). Movement of the sea breeze inland is not uniform, but is dependent in part upon the pre-frontal ABL structure. Three distinct phases appear to exist (e.g. Simpson et al., 1977; Sha et al., 1991) — initial uniform movement followed by deceleration in the early afternoon; acceleration about sunset; deceleration and decay late at night. The first phase corresponds to Clarke's (1984) immature stage when the relative flow is through the isentropes and is far from steady state. The second phase is Clarke's early and late mature stages, when the sea-breeze surge has not reached steady state but, with increased density contrast across the front, acceleration has commenced. During early evening the supply of cool air from the sea ceases, decoupling of the frictional link with the surface occurs and acceleration continues. In the last phase, corresponding with Clarke's early and late degenerate stages, the cold air flattens and spreads inland propagating as an unsteady gravity current.

Abbs and Physick (1992) have reviewed the history of sea-breeze modelling much of which comprises numerical simulations in both two and three space dimensions. Many of the numerical studies utilise hydrostatic mesoscale models on horizontal grids ranging from 2 to 20 km spacing. A number of authors (Pielke, 1972; Martin and Pielke, 1983; Song et al., 1985; Yang, 1991) have concluded that the hydrostatic assumption is valid for grid spacings as small as 1 km, with non-hydrostatic effects tending to weaken the sea breeze when compared to a hydrostatic simulation. Most recently, Sha et al. (1991) used a non-hydrostatic model with a horizontal grid spacing of only 100 m to examine the mixing processes in the head region. This clearly showed the entraining of warmer ambient air into the cooler low-level sea air by the breaking of Kelvin–Helmholz billows.

Land breezes

The land-breeze phenomenon needs to be distinguished from other nighttime flow or circulation phenomema. For example, katabatic or drainage flows usually occur at night under light wind, clear sky conditions wherever there exists sloping terrain, inland or at the coast. In addition, Coriolis effects acting upon the sea-breeze circulation may induce an offshore component during the night.

As with the sea breeze, the land breeze is a shallow boundary-layer phenomenon resulting from the differential surface heating between land and sea that occurs during the night. The induced horizontal pressure gradient produces the land-breeze circulation. This tends to be somewhat weaker and shallower than the sea breeze because there exists no lower heat source to enable penetration of the circulation to heights found with the sea breeze (e.g. see table 23 and fig. 69 in Atkinson, 1981 for observations and theoretical predictions relating to the depths of both sea and land breezes).

In contrast with studies of the sea breeze, the land breeze has not been studied extensively. Indeed, the studies that do exist are often carried out jointly with those of the sea breeze (e.g.

Neumann and Mahrer, 1971; Mizuma and Kakuta, 1974; Mak and Walsh, 1976; Mizuma, 1985). For general discussion relating to the land breeze, the reader is referred to chapter 5 in Atkinson (1981) and chapter 13 in Pielke (1984).

Non-classical mesoscale circulations

General. Sea breezes (and the analogous lake breezes) are associated with significant and spatially coherent horizontal differences in surface temperature, hence surface sensible heat flux. Most importantly they are associated with horizontal pressure differences related directly with temperature differences between distinctive air masses of significant depth. The marine air mass comprises a shallow cool, moist weakly stratified ABL and the terrestrial air mass a deeper, dry convective ABL by day, and (with the sea-breeze front further inland by nightfall) a shallow, dry but stably stratified ABL by night. The air mass density differences are largely dependent on the time history of the surface sensible heat flux across the region.

In analogy to the above, significant spatial variations in the daytime surface sensible heat flux (H) are probably quite common over substantial areas of land. Thermally induced circulations (termed NCMC's to distinguish them from the classical sea-breeze circulation) can be expected under such conditions (e.g. Segal and Arritt, 1992). Following the terminology of these authors, we refer to areas in which H values are suppressed or enhanced relative to the surrounding region as Perturbed Areas (PA's). These are most likely to occur due to spatial variations in surface evaporation or evapotranspiration, solar irradiance absorption or reflection, thermal storage by the subsurface. Perturbed areas inducing significant NCMC's are usually clearly distinguishable from the surroundings, though they are not likely to be as uniform as water surfaces in the sea-breeze case. When they are large enough, the induced circulations may be as intense as a

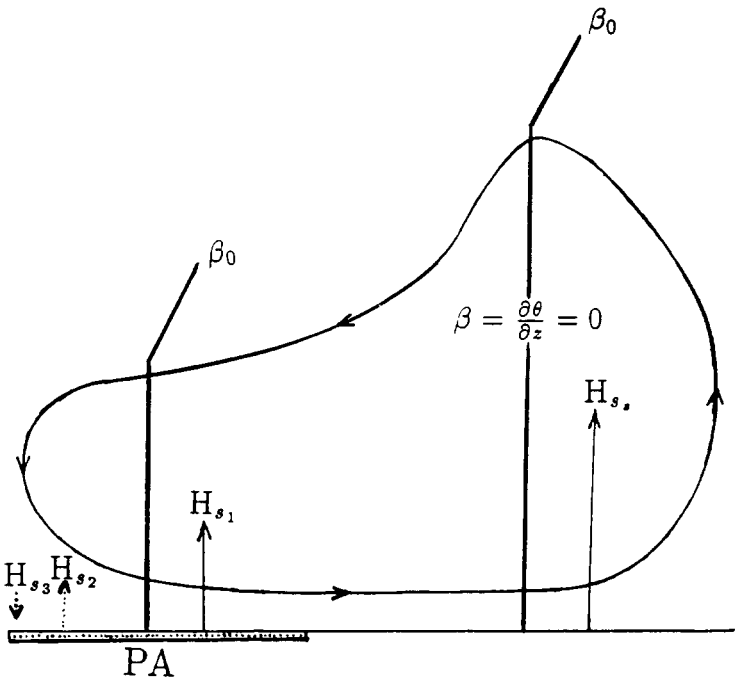

Fig. 18. Illustrative vertical cross section of an NCMC, showing vertical temperature profiles and surface heat fluxes at various locations across the circulation. From Segal and Arritt (1992).

sea breeze. Fig. 18 schematically illustrates a typical NCMC vertical cross section for land situations (from Segal and Arritt, 1992). In most cases, the PA is associated with reduced H to the atmosphere (positive) compared with the region around the PA. In some situations, the sensible heat flux H over the PA may be towards the surface (negative). In both cases, a suppressed CBL or a stable boundary layer will develop over the PA. Figs. 19 and 20 illustrate clearly the differences in temperature above adjacent snow-covered and clear surfaces, and the horizontal variation of H (inferred from a low-flying aircraft) between the two regions (see Segal et al., 1991).

Effects of PA size on generation of NCMC's. The following arguments are largely based on Segal and Arritt (1992). Development of an NCMC requires that the induced pressure-gradient force be sufficient to counteract the imposed ambient wind. We consider an initial Θ stratification $\beta_o = \partial\Theta/\partial z$ which evolves over the surrounding area towards a mixed layer ($\beta \cong 0$) of depth h. Using the Exner function, with $\Pi = c_p T/\Theta$, we can scale the pressure perturbation Π' over the PA as

$$\Pi' = -\int (g\theta'/\hat{\theta}^2)\, dz = -g\beta_o h^2/2\hat{\theta}^2 \qquad (35)$$

where $\hat{\Theta}$ is the average potential temperature within the ABL. Taking a sinusoidal variation in H through the day, and using typical growth models for the CBL (e.g. Tennekes, 1973), we can deduce an expression for the time varying scaled pressure perturbation, viz.

$$\Pi' = -1.2 g\tau H_o[1 - \cos(\pi t/\tau)]/\rho c_p \pi \hat{\theta}^2. \qquad (36)$$

Here, τ is the duration of sunshine hours, H_o is the heat flux over the PA surroundings at noon ($t = 0$ at sunrise). To simplify matters, we assume that the time scale for the development of the pressure perturbation is limited to the advective time scale L/U_g, where L is the minimum width of the PA that produces an NCMC countering the background flow, U_g. We also assume the ideal case of unheated air over the PA ($H = 0$). The pressure perturbation that can be produced during the advective time scale over the PA can be estimated by evaluating Eq. (36) for $t = L/U_g$. It is then assumed that the NCMC will exist if the perturbation pressure gradient at distance L is at

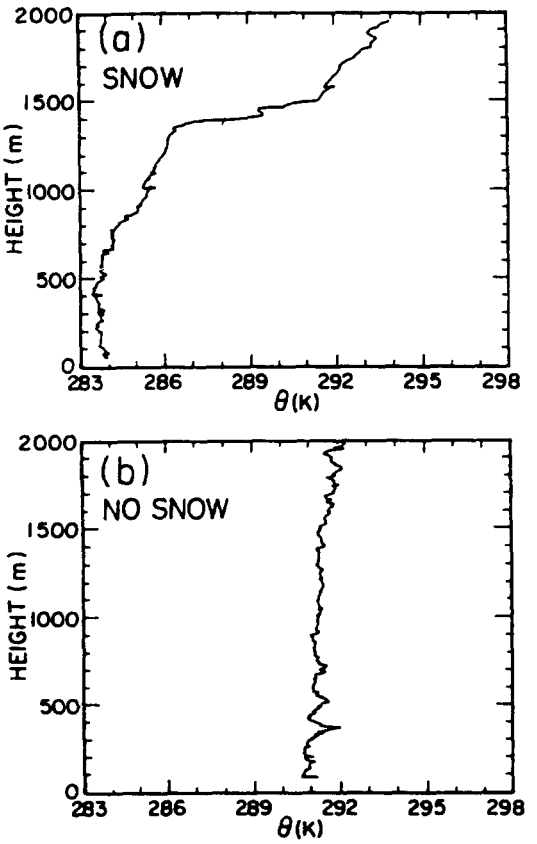

Fig. 19. Vertical profiles of Θ over adjacent snow-covered and bare surfaces — from Segal et al. (1991).

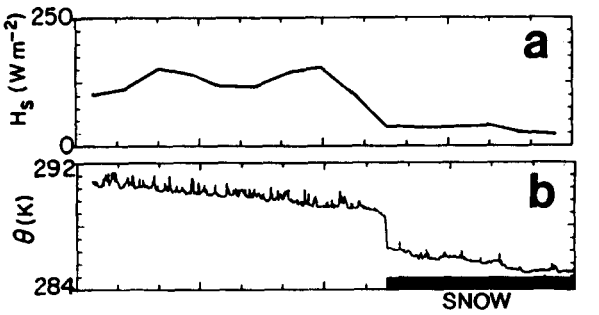

Fig. 20. Horizontal variations of surface heat flux and low-level Θ across a snow- to bare-surface transition — from Segal et al. (1991).

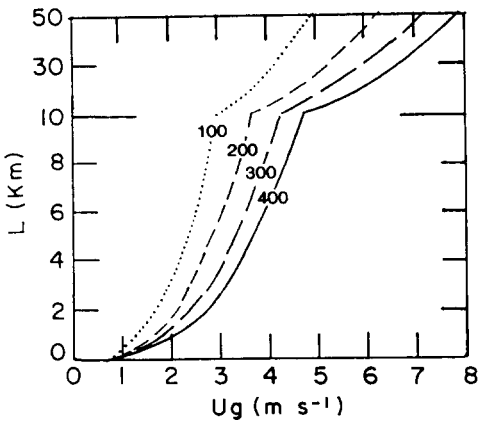

Fig. 21. The minimum PA width, L, needed in order to develop an NCMC flow for a range of opposing synoptic winds, U_g, and several values of the surface heat flux — shown for values from 100 to 400 W m^{-2}. Note the change in ordinate scale at $L = 10$ km. From Segal and Arritt (1992).

least equal to the pressure gradient associated with the opposing background flow U_g. Thus,

$$fU_g = -\hat{\theta}\partial\Pi'/\partial L$$

$$= 1.2gH_o \sin(\pi L/U_g\tau)/\rho c_p\hat{\theta}U_g, \qquad (37)$$

where L provides the minimum PA width for development of an NCMC. Note that the above analysis assumes that the heat flux H over the PA is zero. Where $H > 0$, or the PA has a number of small-scale patches with $H > 0$, the effective H_o in the above equation will have to be reduced. Fig. 21 provides values of L for various combinations of U_g and H_o. It suggests that for $U_g = 3$ ms^{-1} and $H = 100$ Wm^{-2} the impact of the opposing background flow on the suppression of the NCMC is noticeable for $L = 10$ km. Thus, PAs having $L > 10$ km are needed in this case for the NCMC to counter the background flow. For $U_g = 4$ ms^{-1} and the same value of H, suppression of the NCMC occurs for $L < 26$ km. For the ideal extreme case where $H = 400$ Wm^{-2} (typical of mid-summer, inland, dry surrounding conditions with $H = 0$ over the PA), NCMC's would be noticeable with similar background flows for PA's as small as several km (otherwise these results are consistent with Fig. 14, suggesting coherent circulations for surface irregularities of scale > 10 km).

Recent studies on NCMC's

The generation of significant horizontal heat flux differences will lead to differential boundary-layer evolution, and to horizontal temperature gradients throughout the lower atmosphere, resulting in a sea-breeze-like circulation. Sharp contrasts in surface temperature are readily observed from satellite imagery (Segal et al., 1989). The intensity of this circulation will be critically dependent upon the synoptic flow and on the presence of topographically-induced mesoscale flows.

Theoretical and conceptual evaluations of the kinematic and thermodynamic processes associated with NCMC's have been provided, in recent years, by Smith and Mahrt (1981), Anthes (1984), Segal et al. (1984), Pielke and Segal (1986). For example, Anthes (1984) hypothesised that bands of vegetation in semi-arid areas, of optimum spacing ~ 100 km, could, under favourable large-scale conditions, result in enhanced convective precipitation. The basis of this related to (i) increase in low-level moist static energy, (ii) increase in ABL water vapour due to increased evaporation and decreased runoff and (iii) generation of NCMC's associated with the surface inhomogeneities created at this scale by the vegetation. These ideas were broadly confirmed in a numerical study (Han and Anthes, 1988) which showed that strips of dry and wet surface with width and separation ~ 100–200 km can, in a convectively unstable environment with weak synoptic flow and plentiful moisture, initiate convective rainfall.

Numerical model studies by Mahfouf et al. (1987) and Segal et al. (1988) suggested that for prescribed dense, well-watered and extended crop areas, mesoscale circulations of an intensity close to that of a sea breeze may be produced under optimum conditions. In Segal et al. (1988) for example, the presence of vegetation on extensive sloping terrain significantly reduced the upslope flow existing under ideal conditions. Where dense vegetation was introduced into dry-soil areas, and covered an extensive area under optimum envi-

ronmental conditions, circulations close to sea-breeze intensity were developed. The requirement for weak synoptic and upslope flows was emphasised in the observational study of Segal et al. (1989) related to the irrigated crop areas of north east Colorado in the USA. The expected thermally-induced NCMC's were never unambiguously identified, though wind-field changes across the contrast region were observed, and coincident with the thermal and moisture horizontal gradients. It was concluded that the synoptic flow and the daytime, terrain-induced upslope flow combined to mask the NCMC.

7. Numerical modelling and parametrisation schemes

7.1. Models

Numerical solutions of the averaged conservation equations require both a suitable closure scheme to account for the turbulent flux terms, and usually a set of physical parametrisations of the Earth's surface, clouds and radiation. Both one-dimensional ABL models, and two and three-dimensional atmospheric models with horizontal grid scales much greater than the typical ABL length scale ($\sim$ 1 km), utilise ensemble averaged equations. In contrast, in large eddy simulation (LES) models (which potentially represent the best approach to calculating the 3-D, time dependent structure of the ABL), true volume averaging is incorporated. In LES models, subgrid turbulence parametrisation in the limit of small grid scale (relative to the turbulence length scale) is likely to be far simpler, and universally more applicable, than in the ensemble-averaged case. This is so, since large eddies are explicitly resolved and small eddies are likely to take on a more universal character. Unfortunately, in many applications, LES is impracticable — in mesoscale and large-scale models, for example — and emphasis here will be given to the details of closure schemes used with the ensemble averaged equations.

ABL models are usually structured in integral (slab) form, or in high (vertical) resolution form utilising either first-order or higher-order closure.

Integral (slab) models

The integral approach predicts the vertically averaged properties of the ABL, so that details on the vertical profile structure of any property are unavailable. The approach is particularly suited to cases where vertical gradients are small throughout much of the ABL, or where vertically averaged quantities are specifically required. In the former case, the daytime entraining CBL is the best example whilst GCM schemes that have limited vertical resolution are examples of the latter. Closure of the slab equations for both the clear and cloudy ABL requires knowledge of surface and entrainment fluxes and the ABL depth.

High-resolution models

"High resolution" as used here implies multiple levels in the vertical, so allowing the internal structure of the ABL to be evaluated. To solve for the mean fields, the Reynolds flux-divergence term must be approximated at each level. There are two main categories of this type of model: (i) those utilising the ensemble-averaged equations, or volume-averaged equations that approximate ensemble averages because the averaging scale is much greater than the ABL scale and (ii) LES models with volume averaging and explicit representation of the large eddy structure. The ensemble-averaged models may be structured either as a specific ABL model, or as an interactive component of a mesoscale or general circulation model.

Large-eddy simulation models

In these, the averaging volume is sufficiently small that the largest energy containing eddies are resolved explicitly, at least well away from the lower boundary and the overlying inversion layer. This is of paramount importance, since turbulent flows tend to differ from one another mainly in their large-eddy structure whereas the small scales in all turbulent flows tend to be statistically similar. The large eddies are very sensitive to the environment (geometry and stratification), and in particular to the buoyancy forcing. Thus, only the less sensitive small scales need to be parametrised. LES models allow the use of relatively simple

sub-grid closure schemes, including the first- and second-order schemes used in ensemble average models.

Solution of the volume-averaged equations provides variables that are partly random. Thus, to compute mean (in the ensemble sense) vertical profiles of any variable, there is a need to average over a series of horizontal planes and/or over a number of time steps, and/or several runs or simulations. For area-averaged turbulent statistics the total value of the property will be the sum of the resolved and unresolved (parametrised sub-grid) parts.

Before one can determine the surface fluxes, and fluxes throughout the ABL (e.g. through Eqs. 1 to 4), in any model it is often necessary to evaluate a number of surface characteristics. Some properties, including roughness length and albedo, are most likely specified, but this is not generally the case with surface temperature and humidity. If we are dealing with the sea surface, the surface temperature may well be prescribed and the surface humidity taken as the saturated value at this temperature.

7.2. Surface temperature

Numerical models of the atmosphere usually compute the ground surface temperature (T_0) from either a diagnostic form of the surface energy balance (SEB) equation or from a prognostic form, i.e. a rate equation for T_0. The diagnostic form is usually written,

$$R_N - G_0 = H_0 + \lambda E_0 \tag{38a}$$

where R_N is the net radiation and the prognostic form,

$$C_g \partial T_0 / \partial t = R_N - H_0 - \lambda E_0 - G_1 \tag{38b}$$

where C_g is a volumetric heat capacity per unit area of ground, and $G_{0,1}$ are soil heat fluxes at the surface and some small depth respectively.

In the diagnostic case, the ground heat flux may be parametrised very crudely — e.g. as a constant fraction of R_N or by assuming the heat capacity of the ground is zero and setting $G_0 = 0$. Alternatively, it may be computed using a full treatment of soil heat diffusion in a multi-level soil model, with the SEB equation solved iteratively using the Newton–Raphson method (e.g. Jacobs and Brown, 1973; Pielke, 1984 – ch. 11).

In the prognostic case, soil heat flux may be crudely parametrised or even set equal to zero. One method which is widely used is the force-restore method, where the surface temperature is approximated by the temperature of a thin upper layer (e.g. Deardorff, 1978; Dickinson, 1988).

7.3. Surface humidity (soil moisture)

In determining the surface humidity for a bare soil surface, two quite different approaches need to be recognised — interactive and non-interactive. The non-interactive approach means that the surface humidity or soil wetness does not respond to atmospheric forcing in a realistic way, if at all. Several examples can be found in Carson (1982) — see also Garratt (1992 — ch. 8).

The interactive approach allows for feedback between the surface and the prevailing atmospheric conditions. Two common approaches are the "bucket" approach, where surface moisture is identified with that of a single thick slab. Its main shortcoming is that the evaporation does not respond to short-period occurrences of precipitation, which in fact change the moisture content, and hence evaporation, only gradually (Deardorff, 1978). The thick layer is analogous to a bucket which holds, say, 15 cm of water at saturation (it overflows if more water is added from rainfall).

The other approach is force restore, where near-surface soil moisture can be treated in an analogous way to that of surface temperature using a two-layer soil model. As with temperature, the model must represent the rapid response of the near-surface moisture to forcing by precipitation or evaporation and must also include a source of moisture from the deep soil to the surface when there is no precipitation (e.g. Deardorff, 1977). The evaporation may be evaluated as a fraction of the potential rate, where the fraction is dependent on the near-surface soil moisture content (see Noilhan and Planton, 1989).

7.4. Canopy parametrisation

Simple canopy models

The presence of vegetation over an area of ground modulates the evaporation from the soil, and contributes further to the vertical flux of water vapour into the ABL through transpiration. A realistic canopy formulation must ultimately represent the effects of vegetation (averaged over the grid square in a 3D numerical model) upon evaporation, energy partitioning, rainfall interception and soil moisture, as well as albedo and aerodynamic roughness. Inclusion of canopy effects allows the deep soil moisture (in the root zone) to act as a source for evapotranspiration. Except when completely wet, the canopy foliage exerts some degree of physiological control upon the evaporation rate, and the surface humidity becomes indeterminate. Under these conditions, a canopy or surface resistance (conductance) is introduced into the evaporation formulation, and the resistance (conductance) concept is at the heart of most canopy models.

Single-level, canopy formulations are the most appropriate for use in mesoscale and general circulation models, and these will be emphasised here. GCM's, for example, have the option of full canopy or bare soil grid coverage. For partial canopy cover, either as a sparse uniformly distributed cover or as full cover occupying only a fraction of the grid area, more complexity is involved. Discussions on multi-level canopy models, where the variation of fluxes through the canopy is evaluated, can be found in e.g. Finnigan and Raupach (1987) and Raupach (1988).

For a complete vegetation cover, the simplest canopy model uses a constant r_s in Eq. (11b) for evaporation, with r_s values consistent with known bulk stomatal resistances, together with the specified albedo and z_o. In contrast, a complex single-level canopy model contains many parameters with which to evaluate fluxes from the soil beneath the canopy, from open areas between the canopy elements as well as from the foliage itself (e.g. the SiB model of Sellers et al., 1986; the BATS model of Dickinson et al., 1986). In addition the component fluxes are averaged over the grid area in some realistic way. With this approach, quite sophisticated treatments for the surface resistance can be used.

Simple, but realistic, canopy models can be formulated for both isothermal and non-isothermal surfaces. In the isothermal case, both canopy and surface-soil layers are assumed to have the same temperature, but in the non-isothermal approach, the canopy and soil temperatures are

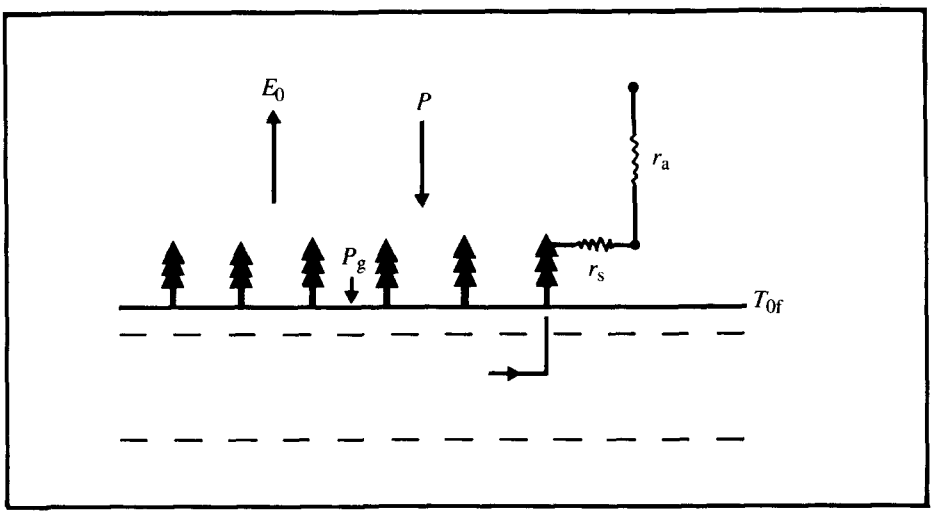

Fig. 22. Schematic representation of an isothermal soil/canopy model (near-surface soil layer and canopy are at temperature T_{0f}). P is precipitation rate.

allowed to differ. These models are essentially 1D formulations applied to a grid area that might comprise either uniform cover (soil or vegetation) or an assumed distribution of patches of bare soil and full canopy.

The isothermal canopy/soil model represents a combined overstorey and soil layer, and assumes that the soil surface and the foliage are at the same temperature T_{of} (Noilhan and Planton, 1989). Fig. 22 sketches the main elements of this approach. The main task is to compute the turbulent fluxes of heat and water vapour, H_o and λE_o respectively, from the canopy to the air. The heat flux is given by the surface-layer relation Eq. (10), with Θ_{of} the canopy (surface) potential temperature, and for evaporation, a distinction is made between dry and wet canopies. Thus, for a wet canopy, evaporation is at the potential rate, and for a dry canopy, with evapotranspiration under physiological control, evaporation is given by Eq. (11b). The relative amounts of dry and wet evaporation are made to depend on the amount of liquid water residing on the foliage, due either to rainfall or dewfall. In addition, the soil moisture depends on precipitation reaching the ground, and so the effects of canopy interception of rainfall should be included.

In order to solve for H_o and E_o, the turbulent fluxes at the top of the canopy, the canopy/soil surface temperature must be evaluated. This is done through a surface energy balance equation, with the soil/canopy system treated as a two-layer structure, and canopy temperature (T_{of}) calculated from the force-restore method.

In contrast, the major features of the non-isothermal canopy/soil model are shown schematically in Fig. 23. In this, the soil surface temperature (T_g) is allowed to differ from the foliage temperature (T_f), resulting in fluxes from both underlying ground (E_g, H_g) and foliage (E_f, H_f) to the atmosphere (Deardorff, 1978). The total fluxes, H_o and E_o, are given by $H_o = H_f + H_g$ and $E_o = E_f + E_g$. In order to solve for the component fluxes, the temperature T_o must be evaluated from a solution of the SEB equations applied at the canopy top (for T_f) and at ground level (for T_g).

Models of partial canopy cover

The canopy formulations discussed above are best applied to vertical exchange from an area of uniform, dense vegetation cover. Their extension to sparse or partial canopy cover is not straightforward, although progress has been made in recent times (Shuttleworth and Wallace, 1985; Shuttleworth and Gurney, 1990). In the real

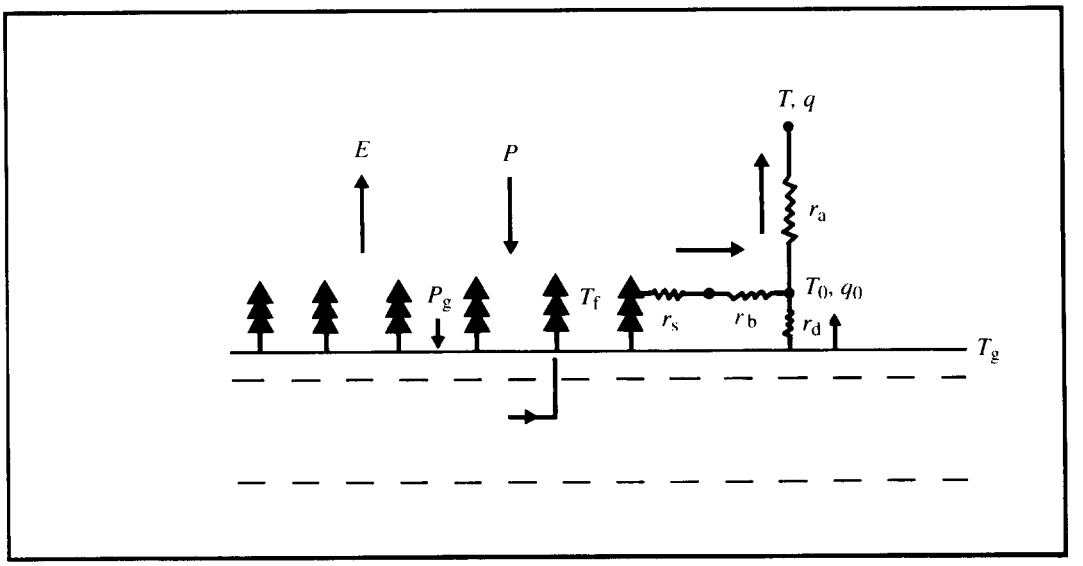

Fig. 23. As in Fig. 22, but for the non-isothermal case — the canopy and upper soil layer are at temperatures T_f and T_g respectively.

world, partial canopy cover is structured in an infinite number of ways, but two extreme structures suffice to illustrate the problem. In the first, a low-density uniform cover exists across the grid area; in the second, the area is comprised of patches of dense canopy and bare soil. From a grid area perspective, the fractional canopy cover σ_f may be the same for each. However, there is obviously a great deal of difference between E_f and E_g when they are the foliage and ground evaporation in a 1D layered system (uniform sparse cover), and when they represent spatially separate areas. Yet in many schemes used in large-scale models, no allowance is made for such differences in sub-grid distribution of vegetation.

Irrespective of the distribution, the simplest schemes evaluate the area-averaged turbulent fluxes as contributions from both canopy and bare soil. One approach assumes a linear combination of these component fluxes, whilst also incorporating suitably modified equations for surface temperature (the SEB), intercepted water and individual fluxes. The total fluxes away from the surface are then given by relations such as

$$H_o = \sigma_f H_{fc} + (1 - \sigma_f) H_{go} \quad (39a)$$

$$E_o = \sigma_f E_{fc} + (1 - \sigma_f) E_{go} \quad (39b)$$

if the isothermal canopy model is used. Here, H_{fc} and E_{fc} are hypothetical fluxes from a full canopy occupying a fraction σ_f of the grid area; H_{go} and E_{go} are fluxes from bare ground. The above relations ensure the correct asymptotic approach as σ_f tends to zero and unity.

Highly detailed, single-level, non-isothermal canopy models have been developed in the last few years for incorporation into GCM's. Their performance should exceed that of their isothermal companions, particularly where temperature differences between foliage and ground are likely to be significant. That is, in partial canopies where shortwave radiation penetrates to the ground. To date, detailed comparisons between model simulations and observations have been few.

7.5. Turbulence closure schemes

We consider here the closure schemes used in association with both the ensemble-averaged equations and volume-averaged equations used in LES modelling. Their principle aim is to allow calculation of vertical fluxes throughout the turbulent ABL, covering the whole range of stabilities.

First-order closure (ensemble models)

First-order closure is often referred to as K-closure and uses a flux-gradient relation such as that expressed by Eqs. (16)–(19), and transfers the problem of the unknown covariances to that of specifying, in a physically realistic manner, the eddy diffusivities.

One-and-a half order closure (ensemble models)

In this approach, the diffusivity is related directly to the turbulent intensity. In fact, it is physically realistic to expect that K will be closely related to the TKE (e), and this is usually assumed. The approach requires solution of the prognostic TKE equation, using either a set of empirical length scales Λ to be specified for each property or a prognostic equation for a master length scale or dissipation rate (e.g. see Holt and Raman, 1988).

Second-order closure (ensemble models)

Second-order closure has been used in turbulence calculations for at least two decades, initially for shear flows and then progressively for ABL modelling in general (see Zeman, 1981). The second-order approach avoids directly the need to parametrise the fluxes using K coefficients in flux-gradient relations. Rather, the covariances and variances are evaluated by solving their respective rate equations. As with one-and-a-half order closure, the complete set of equations must be closed by parametrisation of the pressure covariance, third-order transport and molecular dissipation terms. Usually, second-order closure involves downgradient-diffusion approximations for the third moments, and length-scale assumptions for the dissipation rates (e.g see Mellor and Yamada, 1982: Mellor, 1985).

Non-local closure (ensemble models)

The concept of a first-order nonlocal closure for turbulence becomes attractive in the light of

the failure of local K-theory in the CBL. This closure is nonlocal in the sense of relating the flux of a quantity at a given level to properties at levels throughout the ABL. Two approaches can be found in the literature related to nonlocal flux parametrisation:

(i) in terms of an eddy-diffusivity profile incorporating the nonlocal effects of transport by large eddies in a simplified manner (e.g. Holtslag and Moeng, 1991) — see Section 3.3;

(ii) in terms of transilient turbulence and spectral diffusivity theories, involving an integral closure model which can physically account for the nonlocal effects causing upgradient diffusion and a source-dependent diffusivity in the CBL (e.g. Stull, 1988, ch. 6; Stull, 1993).

The basis of this latter approach rests on the concept of advection by large eddies, such that the concentration of a passive tracer at level i is affected by air mixing in from many adjacent levels. Although the nonlocal approach has a number of attractions, for many purposes local higher-order closure is seen as the alternative to K-theory, particularly with increased use of LES models.

Closures in LES modelling

It is well to note several features of LES models that affect the nature and accuracy of the solution, in addition to the turbulent closure assumption that is adopted. Firstly, the pressure field must be evaluated nonhydrostatically (because of the small grid scales involved) and, secondly, the prescription of boundary conditions at all boundaries has a significant influence on the solution. Surface values of turbulent fluxes are usually determined from standard surface-layer similarity theory.

Values of the subgrid-scale fluxes appearing in the volume-averaged equations (which essentially have the same form as the ensemble-averaged equations) are generally based on K-theory in association with the TKE equation (one-and-a-half order closure), or second-order closure (rarely).

Comments on turbulence closure

The application of first-order closure (K-theory) has been widespread, and an enormous number of K formulations can be found in the literature [see Wipperman's (1973) monograph for work up to the early seventies, for example]. To some extent, this reflects the difficulty of expressing K analytically, or measuring it, above the surface layer. The eddy diffusivity, being a flow property, cannot be accurately prescribed from the outset because it depends on the flow structure to be determined. The principal problem in first-order closure is finding a rational basis for parametrising the diffusivity. Nevertheless, most eddy-viscosity models appear to be quite satisfactory in the neutral and stable ABL. They can reproduce many features of the mean structure, but of course can give no information on the turbulence statistics. In strongly stable conditions, K formulations may fail when decoupling of the flow aloft takes place. More importantly, the local K approach fails in well-mixed layers where mean gradients are close to zero, and usually therefore in the buoyancy dominated convective boundary layer. This has been well demonstrated in the case of bottom-up and top-down diffusion and its impact on mean scalar gradients (Sawford and Guest, 1987). In the CBL, turbulence may become entirely decoupled from the mean gradients and the concept of eddy viscosity based on local properties then becomes physically meaningless. This breakdown seems to be related to the large time scales (the large eddies have a "memory") and the vertical inhomogeneity of the turbulence (Weil, 1990). A nonlocal K approach (Troen and Mahrt, 1986; Holtslag et al., 1990; Holtslag and Boville, 1993) has been used in some modelling applications, as discussed earlier in this paper.

So far as the ABL is concerned, second-order closure is, in principle, less restrictive than integral modelling and it provides information on the vertical distribution of turbulence statistics. Further, second-order models remedy some of the shortcomings of the K-approach (in the CBL, for example) by shifting the problem of closure to higher-order moments. The second-moment equations can also give useful insight into K behaviour, by suitable scaling of the higher-order terms and recasting the steady-state covariance equations into flux-gradient form (e.g. Garratt, 1992; ch. 2).

In many respects, the second-order closure problem reduces to the approximations for the molecular destruction, turbulent transport, and pressure covariance terms in the second-moment equations. The pressure transport term in the TKE equation is typically either neglected or simply absorbed into the turbulent transport term. Closure for the pressure covariance in the flux equations is usually an extended version of Rotta's return-to-isotropy hypothesis.

The turbulent transport (triple correlation) terms are not significant in the neutral and stable ABL, but in the CBL they may dominate the flow dynamics, and the entrainment at the ABL top. The most commonly used closure for the transport terms is the downgradient diffusion model, involving a suitable turbulent length scale (Moeng and Wyngaard, 1989). Finally, many second-order closure models parametrise molecular dissipation rates in terms of velocity and length scales based on standard scaling arguments, thus avoiding the need to carry a rate equation for the dissipation itself.

Closures summarised above were originally developed to model turbulent neutral shear flows, and the associated adjustable constants were mostly obtained from laboratory data. Although transport modelling contains some fundamental problems, these are nowhere as critical as the problems associated with modelling the pressure and dissipation terms. In the case of the transport closure, the downgradient diffusion assumption is clearly inadequate in the CBL where K theory fails. For most atmospheric model applications this is not important because the mean-flow characteristics are not much affected. In fact, LES results have verified the poor performance of the downgradient assumption in the CBL, particularly in the prediction of some turbulent statistics (Moeng and Wyngaard, 1989). The simulation of turbulent second-order statistics using a TKE-dissipation closure approach has also been described by Andren (1991) who compared the results with observations for a range of stabilities.

Another major deficiency lies in the use of length scales, and the fact that all process scales are ultimately related back to one master turbulent scale (l). Determination of this length scale and the associated constants relating it to subsidiary length scales is at the heart of the problem. Although length-scale prescriptions cause fewer problems in modelling, they often oversimplify the physics by constraining the modelled turbulence to an expected state. When multiple scales are present (as in any complex flow, e.g. in the ABL with shear and buoyant forcing; in horizontal flow over a heterogeneous surface) there are advantages in using a differential equation for l. Physically, the alternative approach of using a differential equation for the dissipation rate ϵ has theoretical problems and may not improve the physical realism over the equation for l. But there is evidence of improved simulations of the turbulence in complex flows when using a prognostic equation for l or ϵ rather than the diagnostic (algebraic) approach (e.g. Mellor, 1985; Holt and Raman, 1988).

Second-order modelling of the ABL is still evolving, though the increasing use of volume-averaged models which resolve the large-eddy structure in the ABL (LES models) suggests that the refinements to second-order schemes will not be so crucial in the future. The approach has been called "turbulence engineering" (Wyngaard, 1982), and a wide variety of models can be found in the literature, some based entirely on shear-flow closures and some tuned specifically for buoyancy-dominated turbulence. A recent intercomparison of four LES models based on CBL simulations can be found in Nieuwstadt et al. (1993).

Finally, a number of studies have been reported involving comparisons of simulations of mean and turbulence fields in the ABL which give some insight into the relative performances of first-order (K), one-and-a-half order (TKE) and second-order closure schemes. Thus, the reader is referred to Holt and Raman (1988) — K vs. TKE; Chrobok et al. (1992) — local K vs. nonlocal closure in a cold air outbreak; Smith and Hess (1993) — K vs. second-order closure in the oceans.

7.6. *ABL cloud parametrisation*

In many ABL and larger-scale models, ABL layered cloud is assumed to exist if the ABL top

lies above the local condensation level, i.e. if the relative humidity at $z = h$ is 100%. In many GCM's, low-level stratiform clouds are assumed to be present when the grid-point relative humidity at a specified level in the model exceeds some critical value (about 85–95%). Between this critical value and saturation, fractional cloudiness is allowed to increase according to some empirical relation (e.g. a quadratic relation), becoming full cover at 100% relative humidity. Some schemes then introduce a dependence of cloudiness upon other factors e.g. (i) low-level stability; (ii) the cloud-top entrainment instability.

In both slab and high resolution ABL models, incorporation of moist thermodynamic equations allows the presence of cloud to interact both with the radiation and turbulence fields, and to affect both the surface energy balance for example, and the depth of the ABL.

In many GCM's in use today, the depth of the ABL is not governed by a suitable rate equation and may not even be computed (although it may be set equal to a fixed value). Hence, the presence of stratiform cloud is unaffected by boundary-layer dynamics. Such a non-interactive system can never aspire to simulate the real-world behaviour and distribution of boundary-layer cloud.

Because the ABL controls the evaporation and turbulent redistribution of water substance into the atmosphere, it strongly determines the global distribution of both cumuliform and stratiform clouds. A comprehensive parametrisation of ABL processes for a numerical model of large-scale atmospheric circulations must take into account the interaction of the ABL with clouds. This aspect of the ABL parametrisation problem has an importance comparable to that of determining the turbulent fluxes.

8. Final comments

Recent texts provide the reader with copious information on the atmospheric boundary layer (e.g. Stull, 1988; Sorbjan, 1989; Garratt, 1992), but with the emphasis predominantly on the stationary and time-varying horizontally homogeneous cases. For practical reasons, the continental ABL has received far more attention than the marine case, the clear ABL far more than the cloudy case and the homogeneous or weakly nonhomogeneous ABL far more than the strongly nonhomogeneous case, particularly over complex terrain.

We have attempted to summarise current knowledge on a number of these issues in order that the reader might appreciate the range of problems for which knowledge of boundary-layer processes is an important prerequisite for solutions of these problems.

Much effort has been, and is likely to be, expended on the incorporation of surface and ABL processes in numerical models of the atmosphere. In this context, and possibly for other applications, several areas of research are likely to be given emphasis over the coming years:

(i) area averaging of ABL properties in heterogeneous terrain;

(ii) the structure and behaviour of the strongly time-varying and nonhomogeneous ABL;

(iii) the application of ABL theory over complex terrain, and the influence of sub-grid orography on regional transport;

(iv) the structure, behaviour and parametrisation of the cloudy ABL.

These four areas extend investigation beyond the steady, homogeneous ABL for which extensive theoretical and observational treatments exist. Even so, significant problems still exist in relation to the ideal ABL that have resisted completely acceptable solutions. A good example is the turbulence closure problem, recently discussed by Hasse (1993) who emphasised the lack of a commonly accepted ABL theory analogous to the Monin–Obukhov similarity theory of the surface layer. He noted that the lack of convergence of ABL theory towards a consensus is of practical relevance, e.g. in application of theory within larger-scale atmospheric and oceanic numerical models. His paper was intended to stimulate discussion on whether the ABL community needs to search for an established ABL theory, or whether different theories should be adapted according to the problem to be solved.

All of the above suggests that much still remains to be learnt about the atmospheric boundary layer.

List of symbols

u, v, w	components of velocity along x, y, z axes
x, y, z	Cartesian coordinates (z is the vertical axis)
ρ	density of air
p	pressure
T	absolute temperature
Θ	potential temperature
Θ_v, Θ_e	virtual and equivalent potential temperatures
q	specific humidity
q_l	liquid water content
Θ_o, q_o	surface values of Θ and q
f	Coriolis parameter (N.B. sign(f) = ± 1)
s	generic quantity for u, v, w, T, q
σ_s	standard deviation of s fluctuations
e	mean turbulent kinetic energy
z_o	aerodynamic roughness length
z_T, z_q	roughness lengths for temperature and humidity
β	negative of ratio of entrainment to surface heat fluxes

List of acronyms

ALPEX	Alpine Experiment
AMTEX	Air Mass Transformation Experiment
ARME	Amazon Region Micrometeorology Experiment
ASCOT	Atmospheric Studies in Complex Terrain
AUTAN	Autan wind experiment in France
BOREAS	Boreal Ecosystem Atmosphere Study
CTBL	Cloud topped boundary layer
EFEDA	European Field Experiment in Desertification Threatened Areas
FIFE	First ISLSCP Field Experiment
GARP	Global Atmospheric Research Programme
GATE	GARP Atlantic Tropical Experiment
GCM	General circulation model
HAPEX	Hydrologic Atmospheric Pilot Experiment
ISLSCP	International Satellite Land Surface Climatology Project
JASIN	Joint Air Sea Interaction (Project)
LES	Large-eddy simulation
MESOGERS	Mesoscale experiment in the Gers region
NCMC	Non-classical mesoscale circulation
SESAME	Severe Environmental Storms and Mesoscale Experiment
WMO	World Meteorological Organisation

References

Abbs, D.J., 1986. Sea-breeze interactions along a concave coastline in Southern Australia; Observations and numerical modeling study. Mon. Weather Rev., 114: 831–848.

Abbs, D.J. and Physick, W.L., 1992. Sea-breeze observations and modelling: A review. Aust. Meteorol. Mag., 41: 7–19.

Albrecht, B.A., Penc, R.S. and Schubert, W.H., 1985. An observational study of cloud-topped mixed layers. J. Atmos. Sci., 42: 800–822.

American Meteorological Society, 1990. Symposium on FIFE. Am. Meteorol. Soc., Mass., USA, 180 pp.

Andre, J.C., Goutorbe, J.P. and A. Perrier, 1986. HAPEX-MOBILHY: A hydrologic atmospheric experiment for the study of water budget and evaporation flux at the climatic scale. Bull. Am. Meteorol. Soc., 67: 138–144.

Andre, J.C. et al., 1988. Evaporation over land-surfaces: First results from HAPEX-MOBILHY special observing period. Ann. Geophys., 6(5): 477–492.

Andre, J.C., Bougeault, P. and Goutorbe, J.P., 1990. Regional estimates of heat and evaporation fluxes over non-homogeneous terrain. Examples from the HAPEX-MOBILHY programme. Boundary Layer Meteorol., 50: 77–108.

Andren, A., 1991. A TKE-Dissipation model for the atmospheric boundary layer. Boundary Layer Meteorol., 56: 207–221.

Anthes, R.A., 1984. Enhancement of convective precipitation by mesoscale variation in vegetative covering in semiarid regions. J. Clim. Appl. Meteorol., 23: 541–554.

Arritt, R.W., 1989. Numerical modeling of the offshore extent of sea breezes. Q.J. R. Meteorol. Soc., 115: 547–570.

Arritt, R.W., 1993. Effects of the large-scale flow on characteristic features of the sea breeze. J. Appl. Meteorol., 32: 116–125.

Atkinson, B.W., 1981. Meso-scale Atmospheric Circulations. Academic Press, London, 495 pp.

Banta, R.M., 1984. Daytime boundary-layer evolution over mountaineous terrain. Part I: Observations of the dry circulations. Mon. Weather Rev., 112: 340–356.

Banta, R.M., 1986. Daytime boundary-layer evolution over mountaineous terrain. Part II: Numerical studies of upslope flow duration. Mon. Weather Rev., 114: 1112–1130.

Bechtold, P., Pimty, J.P. and Mascart, P., 1991. A numerical investigation of the influence of large-scale winds on sea-breeze and inland-breeze-type circulations. J. Appl. Meteorol., 30: 1268–1279.

Beljaars, A.C.M. and Holtslag, A.A.M., 1991. Flux parameterization over land surfaces for atmospheric models. J. Appl. Meteorol., 30: 327–341.

Benech, B., Durand, P. and Druilhet, A., 1987. A case study of a non-homogeneous boundary layer (AUTAN 84 experiment). Ann. Geophys., 5B(5): 451–460.

Betts, A.K. and Beljaars, A.C.M., 1993. Estimation of effective roughness length for heat and momentum from FIFE data. Atmos. Res., 30: 251–261.

Betts, A.K. and Ridgway, W., 1989. Climatic equilibrium of the atmospheric convective boundary layer over a tropical ocean. J. Atmos. Sci., 46: 2621–2641.

Betts, A.K., Ball, J.H. and Beljaars, A.C.M., 1993. Comparison between the land surface response of the ECMWF model and the FIFE-1987 data. Q.J. R. Meteorol. Soc., 119(B): 975–1001.

Bougeault, P., Noilhan, J., Lacarrere, P. and Mascart, P., 1991a. An experiment with an advanced surface parameterization in a mesobeta-scale model. Part I: Implementation. Mon. Weather Rev., 119: 2358–2373.

Bougeault, P., Bret, B., Lacarrere, P. and Noilhan, J., 1991b. An experiment with an advanced surface parameterization in a mesobeta-scale model. Part II: The 16 June 1986 simulation. Mon. Weather Rev., 119: 2374–2392.

Britter, R.E. and Simpson, J.E., 1978. Experiments on the dynamics of a gravity current head. J. Fluid Mech., 88: 223–240.

Brost, R.A. and Wyngaard, J.C., 1978. A model study of the stably stratified planetary boundary layer. J. Atmos. Sci., 35: 1427–1440.

Brown, R.A., 1974. Analytical Methods in Planetary Boundary-Layer Modelling. Adam Hilger, London, 148 pp.

Brown, R.A., 1980. Longitudinal instabilities and secondary flows in the planetary boundary layer: A review. Rev. Geophys. Space Phys., 18: 683–697.

Brutsaert, W., 1982. Evaporation into the Atmosphere. Reidel, Dordrecht, 299 pp.

Brutsaert, W. and Kustas, W.L., 1985. Evaporation and humidity profiles for neutral conditions over rugged hilly terrain. J. Clim. Appl. Meteorol., 24: 915–923.

Brutsaert, W. and Kustas, W.L., 1987. Surface water vapour and momentum fluxes under unstable conditions from a rugged-complex area. J. Atmos. Sci., 44: 421–431.

Businger, J.A. and Charnock, H., 1983. Boundary layer structure in relation to larger-scale flow: Some remarks on the JASIN observations. Philos. Trans. R. Soc. London, A308: 445–449.

Carson, D.J., 1982. Current parameterizations of land-surface processes in atmospheric general circulation models. In: P.S. Eagleson (Editor), Land Surface Processes in Atmospheric General Circulation Models. C.U.P., London, pp. 67–108.

Caughey, S.J., Wyngaard, J.C. and Kaimal, J.C., 1979. Turbulence in the evolving stable boundary layer. J. Atmos. Sci., 36:.1041–1052.

Charnock, H. and Pollard R.T., (Editors), 1983. Results of the Royal Society Joint Air–Sea Interaction Project (JASIN). R. Soc., London, 229 pp.

Chou, S.H., 1993. A comparison of airborne eddy correlation and bulk aerodynamic methods for ocean-air turbulent fluxes during cold-air outbreaks. Boundary Layer Meteorol., 64: 75–100.

Chrobok, G., Raasch, S. and Etling, D., 1992. A comparison of local and non-local turbulence closure methods for the case of a cold air outbreak. Boundary Layer Meteorol., 58: 69–90.

Clarke, R.H., 1970. Recommended methods for the treatment of the boundary layer in numerical models. Aust. Meteorol. Mag., 18: 51–71.

Clarke, R.H., 1984. Colliding sea-breezes and the creation of internal atmospheric bore waves: Two dimensional numerical sudies. Aust. Meteorol. Mag., 32: 207–226.

Clarke, R.H., 1990. Modelling mixed-layer growth in the Koorin experiment. Aust. Meteorol. Mag., 38: 227–234.

Clarke, R.H., Dyer, A.J., Brook, R.R., Reid, D.G. and Troup, A.J., 1971. The Wangara Experiment: boundary-layer data. Tech. Pap., 19. Div. Meteorol. Phys., CSIRO, Australia, 21 pp.

Clarke, R.H. and Brook, R.R., 1979. The Koorin Expedition — Atmospheric Boundary Layer Data over Tropical Savannah Land. Dep. Science, Canberra, 359 pp.

Deardorff, J.W., 1972. Parameterization of the planetary boundary layer for use in general circulation Models. Mon. Weather Rev., 100: 93–106.

Deardorff, J.W., 1974. Three-dimensional numerical study of the height and mean structure of a heated planetary boundary layer. Boundary Layer Meteorol., 7: 81–106.

Deardorff, J.W., 1977. A parameterization of ground-surface moisture content for use in atmospheric prediction models. J. Appl. Meteorol., 16: 1182–1185.

Deardorff, J.W., 1978. Efficient prediction of ground surface temperature and moisture, with inclusion of a layer of vegetation. J. Geophys. Res., 83(C4): 1889–1903.

Deardorff, J.W., Ueyoshi, K. and Han, Y.-J., 1984. Numerical study of terrain-induced mesoscale motions and hydrostatic form drag in a heated, growing mixed layer. J. Atmos. Sci., 41: 1420–1441.

Dickinson, R.E., 1988. The force-restore model for surface temperature and its generalizations. J. Climate, 1: 1086–1097.

Dickinson, R.E., Henderson-Sellers, A., Kennedy, P.J. and Wilson, M.F., 1986. Biosphere–Atmosphere Transfer Scheme (BATS) for the NCAR Community Climate Model. NCAR Technical Note NCAR/TN-275+STR, 69 pp.

Durand, P., Druilhet, A., Hedde, T. and Benech, B., 1987. Aircraft observations of the structure of the boundary layer over a rugged hilly region (MESOGERS 84 experiment). Ann. Geophys., 5B(5), 441–450.

Durand, P., Briere, S. and Druilhet, A., 1989. A sea–land transition observed during the COAST experiment. J. Atmos. Sci., 46: 96–116.

Egger, J., 1987a. Simple models of the valley-plain circulation. Part I: Minimum resolution model. Meteorol. Atmos. Phys., 36: 231–242.

Egger, J., 1987b. Simple models of the valley-plain circulation. Part II: Flow resolving model. Meteorol. Atmos. Phys., 36: 243–254.

Etling, D. and Brown, R.A., 1993. Roll vortices in the planetary boundary layer: A review. Boundary Layer Meteorol., 65: 215–248.

Fiedler, B.H., 1984. An integral closure model for the vertical turbulent flux of a scalar in a mixed layer. J. Atmos. Sci., 41: 674–680.

Finnigan, J.J. and Raupach, M.R., 1987. Transfer processes in plant canopies in relation to stomatal characteristics. In: E. Zeiger, G. Farquhar and I. Cowan (Editors), Stomatal Function. Stanford Univ. Press, Calif., pp. 385–429.

Francey, R.J. and Garratt, J.R., 1978. Eddy flux measurements over the ocean and related transfer coefficients. Boundary Layer Meteorol., 14: 153–166.

Garratt, J.R., 1980. Surface influence upon vertical profiles in the atmospheric near-surface layer. Q.J. R. Meteorol. Soc., 106: 803–819.

Garratt, J.R., 1982. Observations in the nocturnal boundary layer. Boundary Layer Meteorol., 22: 21–48.

Garratt, J.R., 1983. Surface influence upon vertical profiles in the nocturnal boundary layer. Boundary Layer Meteorol., 26: 69–80.

Garratt, J.R., 1987. The stably stratified internal boundary layer for steady and diurnally varying offshore flow. Boundary Layer Meteorol., 38: 369–394.

Garratt, J.R., 1990. The internal boundary layer — A review. Boundary Layer Meteorol., 50: 171–203.

Garratt, J.R., 1992. The Atmospheric Boundary Layer. Cambridge Univ. Press, Cambridge, U.K., 316 pp.

Garratt, J.R. and Hicks, B.B., 1973. Momentum, heat and water vapour transfer to and from natural and artificial surfaces. Q.J. R. Meteorol. Soc., 99: 680–687.

Garratt, J.R. and Physick, W.L., 1985. The inland boundary layer at low latitudes: II. Sea breeze influences. Boundary Layer Meteorol., 33: 209–231.

Garratt, J.R. and Ryan, B.F., 1989. The structure of the stably stratified internal boundary layer in offshore flow over the sea. Boundary Layer Meteorol., 47: 17–40.

Garratt, J.R. and Pielke, R.A., 1989. On the sensitivity of mesoscale models to surface-layer parameterization constants. Boundary Layer Meteorol., 48: 377–387.

Garratt, J.R., Hicks, B.B. and Valigura, R.A., 1993. Comments on "The roughness length for heat and other vegetation parameters for a surface of short grass". J. Appl. Meteorol., 32: 1301–1303.

Grant, A.L.M. and Mason, P.J., 1990. Observations of boundary layer structure over complex terrain. Q.J. R. Meteorol. Soc., 116: 159–186.

Gudiksen, P.H. and Dickerson, M.H. (Editors), 1983. Executive summary: Atmospheric Studies in Complex Terrain. Technical Progress Report FY-1979 through FY-1983 (August 1983). Lawrence Livermore National Lab, Univ. Calif., 94550, 41 pp.

Hafner, T.A. et al., 1987. Boundary layer aspects and elevated heat source effects of the Alps. Meteorol. Atmos. Phys., 36: 61–73.

Han, Y.J. et al., 1982. Numerical study of terrain-induced mesoscale motions in a mixed layer. J. Atmos. Sci., 39: 2464–2476.

Han, Y. and Anthes, R.A., 1988. The effect of variations in surface moisture on mesoscale circulations. Mon. Weather Rev., 116: 192–208.

Hasse, L., 1993. Turbulence closure in boundary-layer theory — An invitation to debate. Boundary Layer Meteorol., 65: 249–254.

Haugen, D.A. (Editor), 1973. Workshop on Micrometeorology. Am. Meteorol. Soc., Boston, Mass., 392 pp.

Hennemuth, B., 1987. Heating of a small alpine valley. Meteorol. Atmos. Phys., 36: 287–296.

Hess, G.D., 1992. Observations and scaling of the atmospheric boundary layer. Aust. Meteorol. Mag., 41: 79–99.

Holt, T. and Raman, S., 1988. A review and comparative evaluation of multilevel boundary layer parameterizations for first-order and turbulent kinetic energy closure schemes. Rev. Geophys., 26: 761–780.

Holtslag, A.A.M. and Moeng, C.-H., 1991. Eddy diffusivity and countergradient transport in the convective atmospheric boundary layer. J. Atmos. Sci., 48: 1690–1698.

Holtslag, A.A.M. and Boville, B.A., 1993. Local versus nonlocal boundary-layer diffusion in a global climate model. J. Climate, 6: 1825–1842.

Holtslag, A.A.M., De Bruin, E.I.F. and Pan, H.L., 1990. A high resolution air mass transformation model for short-range weather forecasting. Mon. Weather Rev., 118: 1561–1575.

Hopwood, W.P., 1991. Radiosonde observation of boundary layer characteristics over two types of complex terrain. Annal. Geophys., Suppl. Vol. 9: 224–225.

Hsu, S.A., 1983. On the growth of a thermally modified boundary layer by advection of warm air over a cooler sea. J. Geophys. Res., 88 (C1): 771–774.

Hsu, S.A., 1986. A note on estimating the height of the convective internal boundary layer near shore. Boundary Layer Meteorol., 35: 311–316.

Hunt, J.C.R., Leibovich, S. and Richards, K.J., 1988a. Turbu-

lent shear flow over low hills. Q.J. R. Meteorol. Soc., 114: 1435–1470.

Hunt, J.C.R., Richards, K.J. and Brighton, P.W.M., 1988b. Stably stratified shear flow over low hills. Q.J. R. Meteorol. Soc., 114: 859–886.

ISLSCP, 1993. ISLSCP Workshop Report, Remote Sensing of the Land Surface for Studies of Global Change. P.J. Sellers (Editor), NASA/GSFC, Greenbelt, MD.

Izumi, Y., 1971. Kansas 1968 Field Program Data Report. Air Force Cambridge Res. Lab., Bedford, Mass., AFCRL-72-0041. Environ. Res. Pap., 379, 79 pp.

Izumi, Y. and Caughey, S.J., 1976. Minnesota 1973 Atmospheric Boundary Layer Experimental Data Report. Air Force Cambridge Res. Pap., 547.

Jackson, P.S. and Hunt, J.C.R., 1975. Turbulent wind flow over a low hill. Q.J. R. Meteorol. Soc., 101: 929–955.

Jacobs, C.A. and Brown, P.S., 1973. An investigation of the numerical properties of the surface heat-balance equation. J. Appl. Meteorol., 12: 1069–1072.

Kader, B.A. and Yaglom, A.M., 1990. Mean fields and fluctuation moments in unstably stratified turbulent boundary layers. J. Fluid Mech., 212: 637–662.

Kaimal, J.C. and Finnigan, J.J., 1993. Atmsopheric Boundary Layer Flows. Oxford University Press, U.K., 282 pp.

Kaimal, J.C., Wyngaard, J.C., Izumi, Y. and Cote, O.R., 1972. Spectral characteristics of surface layer turbulence. Q.J. R. Meteorol. Soc., 98: 563–589.

Kaimal, J.C., Wyngaard, J.C., Haugen, D.A., Cote, O.R., Izumi, Y., Caughey, S.J. and Readings, C.J., 1976. Turbulence structure in the convective boundary layer. J. Atmos. Sci., 33: 2152–2169.

Kraus, H., 1982. PUKK: A meso-scale experiment at the German North Sea coast. Beitr. Phys. Atmos., 55: 370–382.

Kraus, H., Hacker, J.M. and Hartmann, J., 1990. An observational aircraft-based study of sea-breeze frontogenesis. Boundary Layer Meteorol., 53: 223–265.

Kondo, H., 1990. A numerical experiment on the interaction between sea breeze and valley wind to generate the so-called "Extended sea breeze". J. Meteorol. Soc. Jpn., 68: 435–446.

Kuettner, J.P. and Holland, J., 1969. The BOMEX Project. Bull. Am. Meteorol. Soc., 50: 394–402.

Kuettner, J.P. and Parker, D.E., 1976. GATE: Report on the field phase. Bull. Am. Meteorol. Soc., 57: 11–30.

Kustas, W.P. and Brutsaert, W., 1986. Wind profile constants in a neutral atmospheric boundary layer over complex terrain. Boundary Layer Meteorol., 34: 35–54.

LeMone, M.A., 1980. The marine boundary layer. In: Workshop on the Planetary Boundary Layer. Am. Meteorol. Soc., Boston, Mass., 182–234.

Lenschow, D.H. and Agee, E.M., 1976. Preliminary results from the air mass transformation experiment (AMTEX). Bull. Am. Meteorol. Soc., 57: 1346–1355.

Lenschow, D.H. (Editor), 1986. Probing the Atmospheric Boundary Layer. Am. Meteorol. Soc., Boston, Mass., 269 pp.

Lenschow, D.H, Li, X.S., Zhu, C.J. and Stankov, B.B., 1988a. The stably stratified boundary layer over the Great Plains. I. Mean and turbulence structure. Boundary Layer Meteorol., 42: 95–121.

Lenschow, D.H., Zhang, S.F. and Stankov, B.B., 1988b. The stably stratified boundary layer over the Great Plains. II. Horizontal variations and spectra. Boundary Layer Meteorol., 42: 123–135.

Lettau, H.H. and Davidson, B., 1957. Exploring the Atmosphere's First Mile, Vols. 1-2. Pergamon Press, New York.

Lumley, J.L. and Panofsky, H.A., 1964. The Structure of Atmospheric Turbulence. Wiley, Interscience, New York, 239 pp.

Mahfouf, J.F., Richard, E. and Mascart, P., 1987. The influence of soil and vegetation on the development of mesoscale circulations. J. Climate Appl. Meteorol., 26: 1483–1495.

Mahrt, L., 1987. Grid-averaged surface fluxes. Mon. Weather Rev., 115: 1550–1560.

Mahrt, L. and Ek, M., 1993. Spatial variability of turbulent fluxes and roughness lengths in HAPEX-MOBILHY. Boundary Layer Meteorol., 65: 381–400.

Mak, M.K. and Walsh, J.E., 1976. On the relative intensities of sea and land breezes. J. Atmos. Sci., 33: 242–251.

Manins, P.C., 1982. The daytime planetary boundary layer: A new interpretation of Wangara data. Q.J. R. Meteorol. Soc., 108: 689–705.

Martin, C.L. and Pielke, R.A., 1983. The adequacy of the hydrostatic assumption in sea-breeze modeling over flat terrain. J. Atmos. Sci., 40: 1472–1481.

Mason, P.J. and Thomson, D.J., 1987. Large-eddy simulations of the neutral-static-stability planetary boundary layer. Q.J. R. Meteorol. Soc., 113: 413–443.

McBean, G.A., Bernhardt, K., Bodin, S., Litynska, Z., Van Ulden, A.P. and Wyngaard, J.C., 1979. The Planetary Boundary Layer. WMO Tech. Note, 165, Geneva, 201 pp.

McNaughton, K.G. and Spriggs, T.W., 1989. An evaluation of the Priestley and Taylor equation and complementary relationship using results from a mixed-layer model of the convective boundary layer. IAHS Publ., 177: 89–104.

McNider, R.T. and Pielke, R.A., 1984. Numerical simulation of slope and mountain flows. J. Clim. Appl. Meteorol., 23: 1441–1453.

Mehrez, M.B., Taconet, O., Vidal-Madjar, D. and Valencogne, C., 1992a. Estimation of stomatal resistance and canopy evaporation during the HAPEX-MOBILHY experiment. Agric. Forest Meteorol., 58: 285–313.

Mehrez, M.B., Taconet, O., Vidal-Madjar, D. and Sucksdorff, Y., 1992b. Calibration of an energy flux model over bare soils during the HAPEX-MOBILHY experiment. Agric. Forest Meteorol., 58: 257–283.

Mellor, G.L., 1985. Ensemble average, turbulence closure. Adv. Geophys., 28B: 345–358.

Mellor, G.L. and T. Yamada, 1982. Development of a turbulence closure model for geophysical fluid problems. Rev. Geophys. Space Phys., 20: 851–875.

Mizuma, M., 1985. An observational study of land and sea breezes in the southern part of the Osaka District. Annu. Rep. Res. Reactor Inst., Kyoto Univ., 18: 68–81.

Mizuma, M. and Kakuta, M., 1974. An observational study of

land and sea breezes in the Tokai village area. J. Meteorol. Soc. Jpn., 52: 417–427.

Moeng, C.-H. and Wyngaard, J.C., 1984. Statistics of conservative scalars in the convective boundary layer. J. Atmos. Sci., 41: 3161–3169.

Moeng, C.-H. and Wyngaard, J.C., 1989. Evaluation of turbulent transport and dissipation closures in second-order modeling. J. Atmos. Sci., 46: 2311–2330.

Mulhearn, P.J., 1981. On the formation of a stably stratified internal boundary layer by advection of warm air over a cooler sea. Boundary Layer Meteorol., 21: 247–254.

Nakane, H. and Sasano, Y., 1986. Structure of a sea-breeze front revealed by scanning lidar observation. J. Meteorol. Soc. Jpn., 64: 787–792.

Neumann, R.J. and Mahrer, B.A., 1971. A theoretical study of the land and sea breeze circulation. J. Atmos. Sci., 28: 532–542.

Nicholls, S., 1985. Aircraft observations of the Ekman layer during the joint air–sea interaction experiment. Q.J. R. Meteorol. Soc., 111: 391–426.

Nicholls, S. and Leighton, J., 1986. An observational study of the structure of stratiform cloud sheets, Part I: Structure. Q.J. R. Meteorol. Soc., 112: 431–460.

Nieuwstadt, F.T.M., 1984. The turbulent structure of the stable, nocturnal boundary layer. J. Atmos. Sci., 41: 2202–2216.

Nieuwstadt, F.T.M., 1985. A model for the stationary, stable boundary layer. In: J.C.R. Hunt (Editor), Turbulence and Diffusion in Stable Environments. Clarendon Press, Oxford, pp. 149–179.

Nieuwstadt, F.T.M. and Tennekes, H., 1981. A rate equation for the nocturnal boundary-layer height. J. Atmos. Sci., 38: 1418–1428.

Nieuwstadt, F.T.M. and van Dop, H. (Editors), 1982. Atmospheric Turbulence and Air Pollution Modelling. Reidel, Dordrecht, 358 pp.

Nieuwstadt, F.T.M., Mason, P.J., Moeng, C-H. and Schumann, U., 1993. large-eddy simulation of the convective boundary layer: A comparison of four computer codes. In: F. Furst et al. (Editors), Turbulent Shear Flows 8. Springer, Berlin, pp. 343–368.

Noilhan, J. and Planton, S., 1989. A simple parameterization of land surface processes for meteorological models. Mon. Weather Rev., 117: 536–549.

Noilhan, J., Lacarrere, P. and Bougeault, P., 1991. An experiment with an advanced surface parameterization in a mesobeta-scale model. Part III: Comparison with the HAPEX-MOBILHY dataset. Mon. Weather Rev., 119: 2393–2413.

Palmen, E. and Newton, C.W., 1969. Atmospheric Circulation Systems. Academic Press, New York, 603 pp.

Physick, W.L., 1980. Numerical experiments on the inland penetration of the sea breeze. Q.J. R. Meteorol. Soc., 106: 735–746.

Pielke, R.A., 1972. Comparison of a Hydrostatic and an Anelastic Dry Shallow Primitive Equation Model. NOAA Tech. Mem., ERL OD-13, NOAA ERL, Office of the Director, Boulder, Col., 47 pp.

Pielke, R.A., 1984. Mesoscale Meteorological Modeling. Academic Press, New York, 612 pp.

Pielke, R.A. and M. Segal, 1986. Mesoscale circulations forced by differential heating. In: P. Ray (Editor), Mesoscale Meteorology and Forecasting. Am. Meteorol. Soc., pp. 516–548.

Pinty, J.P., Mascart, P., Bechtold, P. and Rosset, R., 1992. An application of the vegetation–atmosphere coupling concept to the HAPEX-MOBILHY experiment. Agric. Forest Meteorol., 61: 253–279.

Priestley, C.H.B., 1959. Turbulent Transport in the Lower Atmosphere. Univ. Chicago Press, Chicago, 130 pp.

Priestley, C.H.B. and Taylor, R.J., 1972. On the assessment of surface heat flux and evaporation using large-scale parameters. Mon. Weather Rev., 100: 81–92.

Raupach, M.R., 1988. Canopy transport processes. In: W.L. Steffen and O.T. Denmead (Editor), Flow and Transport in the Natural Environment: Advances and Applications. Springer, New York, pp. 95–127.

Raupach, M.R., Thom, A.S. and Edwards, I., 1980. A wind-tunnel study of turbulent flow close to regularly arrayed rough surfaces. Boundary Layer Meteorol., 18: 373–397.

Sawford, B.L. and Guest, F.M., 1987. Lagrangian stochastic analysis of flux-gradient relationships in the convective boundary layer. J. Atmos. Sci., 44: 1152–1165.

Segal, M. and Arritt, R.W., 1992. Nonclassical mesoscale circulations caused by surface sensible heat-flux gradients. Bull. Am. Meteorol. Soc., 73: 1593–1604.

Segal, M., Pielke, R.A. and Mahrer, Y., 1984. Evaluation of surface sensible heat flux effects on the generation and modification of mesoscale circulations. Proc. Second Int. Symp. on Nowcasting. E.S.A., Norrkoping, Sweden, pp. 263–269.

Segal, M., Avissar, R., McCumber, M.C. and Pielke, R.A., 1988. Evaluation of vegetation effects on the generation and modification of mesoscale circulations. J. Atmos. Sci., 45: 2268–2292.

Segal, M., Schreiber, W., Kallos, G., Garratt, J.R., Rodi, A., Weaver, J. and Pielke, R.A., 1989. The impact of crop areas in northeast colorado on midsummer mesoscale thermal circulations. Mon. Weather Rev., 117: 809–825.

Segal, M., Cramer, J.H., Pielke, R.A., Garratt, J.R. and Hildebrand, P., 1991. Observational evaluations of the snow breeze. Mon. Weather Rev., 119: 412–424.

Sellers, P.J., Mintz, Y., Sud, Y.C. and Dalcher, A., 1986. A simple biosphere model (SiB) for use within general circulation models. J. Atmos. Sci., 43: 505–531.

Sellers, P.J., Hall, F.G., Asrar, G., Strebel, D.E. and Murphy, R.E., 1988. The first ISLSCP field experiment (FIFE). Bull. Am. Meteorol. Soc., 69: 22–27.

Sha, W., Kawamura, T. and Ueda, H., 1991. A numerical study on sea/land breezes as a gravity current: Kelvin–Helmholtz billows and inland penetration of the sea-breeze front. J. Atmos. Sci., 48: 1649–1665.

Sheppard, P.A., Charnock, H. and Francis, J.R.D., 1952. Observations of the westerlies over the sea. Q.J. R. Meteorol. Soc., 78: 563–582.

Shuttleworth, W.J., 1991. The modellion concept. Rev. Geophys., 29: 585–606.

Shuttleworth, W.J. and Gurney, R.J., 1990. The theoretical relationship between foliage temperature and canopy resistance in sparse crops. Q.J. R. Meteorol. Soc., 116: 497–519.

Shuttleworth, W.J. and Wallace, J.S., 1985. Evaporation from sparse crops — An energy combination theory. Q.J. R. Meteorol. Soc., 111: 839–855.

Simpson, J.E., 1969. A comparison between laboratory and atmsopheric density currents. Q.J. R. Meteorol. Soc., 95: 758–765.

Simpson, J.E., 1972. Effects of the lower boundary on the head of a gravity current. J. Fluid Mech., 53: 759–768.

Simpson, J.E. and Britter, R.E., 1979. The dynamics of the head of a gravity current advancing over a horizontal surface. J. Fluid Mech., 94: 477–495.

Simpson, J.E., Mansfield, D.A. and Milford, J.R., 1977. Inland penetration of sea-breeze fronts. Q.J. R. Meteorol. Soc., 103: 47–76.

Smith, R.B., 1986. Current status of ALPEX research in the United States. Bull. Am. Meteorol. Soc., 67: 310–318.

Smith, B. and Mahrt, L., 1981. A study of boundary layer pressure adjustments. J. Atmos. Sci., 18: 334–346.

Smith, N.R. and Hess, G.D., 1993. A comparison of vertical eddy mixing parameterizations for equatorial ocean models. J. Phys. Oceanog., 23: 1823–1830.

Song, J.L., Pielke, R.A., Segal, M., Arritt, R.W. and Kessler, R.C., 1985. A method to determine nonhydrostatic effects within subdomains in a mesoscale model. J. Atmos. Sci., 42: 2110–2120.

Sorbjan, Z., 1989. Structure of the Atmospheric Boundary Layer. Prentice Hall, New Jersey, 317 pp.

Stewart, R.W., 1979. The Atmospheric Boundary Layer. WMO-No. 523, World Meteorological Organization, 44 pp.

Stull, R.B., 1984. Transilient turbulence theory. Part I: The concept of eddy mixing across finite distances. J. Atmos. Sci., 41: 3351–3367.

Stull, R.B., 1985. A fair-weather cumulus cloud classification scheme for mixed layer studies. J. Clin. Appl. Meteorol., 24: 49–56.

Stull, R.B., 1988. An Introduction to Boundary Layer Meteorology. Kluwer, Dordrecht, 666 pp.

Stull, R.B., 1993. Review of non-local mixing in turbulent atmospheres: Transilient turbulence theory. Boundary Layer Meteorol., 62: 21–96.

Stull, R.B. and Driedonks, A.G.M., 1987. Applications of the transilient turbulence parameterization to atmospheric boundary-layer simulations. Boundary Layer Meteorol., 40: 209–239.

Sugita, M. and Brutsaert, W., 1992. The stability functions in bulk similarity formulation for the unstable boundary layer. Boundary Layer Meteorol., 61: 65–80.

Sutton, O.G., 1953. Micrometeorology. McGraw-Hill, London, 333 pp.

Swinbank, W.C., 1968. A comparison between predictions of dimensional analysis for the constant flux layer and observations in unstable conditions. Q.J. R. Meteorol. Soc., 94: 460–467.

Taylor, P.A. and Tuenissen, H.W., 1987. The Askervein Hill Project: Overview and background data. Boundary Layer Meteorol., 39: 15–39.

Taylor, P.A., Mason, P.J. and Bradley, E.F., 1987. Boundary-layer flow over low hills. Boundary Layer Meteorol., 39: 107–132.

Tennekes, H., 1973. Similarity laws and scale relations in planetary boundary layers, ch. 5. In: A. Haugen (Editor), Workshop on Micrometeorology. Am. Meteorol. Soc., Boston, Mass., 177–216.

Tennekes, H., 1982. Similarity relations, scaling laws and spectral dynamics. In: F.T.M. Nieuwstadt and H. van Dop (Editors), Atmospheric Turbulence and Air Pollution Modelling. Reidel, Dordrecht, pp. 37–68.

Tennekes, H. and Lumley, J.L., 1972. A First Course in Turbulence. M.I.T. Press, Cambridge, Mass., 300 pp.

Troen, I. and Mahrt, L., 1986. A simple model of the atmospheric boundary layer: Sensitivity to surface evaporation. Boundary Layer Meteorol., 37: 129–148.

Venkatram, A., 1977. A model of internal boundary-layer development. Boundary Layer Meteorol., 11: 419–437.

Vergeiner, I. and Dreiseitl, E., 1987. Valley winds and slope winds — Observations and elementary thoughts. Meteorol. Atmos. Phys., 36: 264–286.

Walmsley, J.L., 1992. Proposal for new PBL resistance laws for neutrally-statified flow. Boundary Layer Meteorol., 60: 271–306.

Weil, J.C., 1990. A diagnosis of the asymmetry in top-down and bottom-up diffusion using a Lagrangian stochastic model. J. Atmos. Sci., 47: 501–515.

Weill, A., Baudon, F., Resbraux, G., Mazaudier, C., Klapisz, C. and Driedonks, A.G.M., 1985. A mesoscale shear-convective organization and boundary-layer modification: An experimental study performed with acoustic Doppler sounders during the COAST experiment. Proc. 2nd Conf. Mesoscale Processes, Am. Meteorol. Soc., Boston, Mass.

Weill, A. et al., 1988. The "Mesogers 84" Experiment: A report. Boundary Layer Meteorol., 42: 251–264.

Wipperman, F., 1973. The Planetary Boundary Layer of the Atmosphere. Dtsch. Wetterd., Offenbach, 346 pp.

Wood, N. and P.J. Mason, 1993. The pressure force induced by neutral, turbulent flow over hills. Q.J. R. Meteorol. Soc., 119: 1233–1267.

Wyngaard, J.C., (Editor), 1980. Workshop on the Planetary Boundary Layer. Am. Meteorol. Soc., Boston, Mass., 322 pp.

Wyngaard, J.C., 1982. boundary-layer modeling. In: F.T.M. Nieuwstadt and H. van Dop (Editors), Atmospheric Turbulence and Air Pollution Modelling. Reidel, Dordrecht, pp. 69–158.

Wyngaard, J.C. and Brost, R.A., 1984. Top-down and bottom-

up diffusion of a scalar in the convective boundary layer. J. Atmos. Sci., 41: 102–112.
Yamada, T., 1976. On the similarity functions A, B and C of the planetary boundary layer. J. Atmos. Sci., 33: 781–793.
Yan, H. and Anthes, R.A., 1988. The effect of variations in surface moisture on mesoscale circulations. Mon. Weather Rev., 116: 192–208.
Yang, X., 1991. A study of nonhydrostatic effects in idealized sea breeze systems. Boundary Layer Meteorol., 54: 183–208.
Zeman, O., 1981. Progress in the modeling of planetary boundary layers. Annu. Rev. Fluid Mech., 13: 253–272.
Zilitinkevich, S.S., 1970. Dynamics of the Atmospheric Boundary Layer. Hydrometeorol., Leningrad, translated by C. Long, 239 pp.
Zilitinkevich, S.S., 1972. On the determination of the height of the Ekman boundary layer. Boundary Layer Meteorol., 3: 141–145.

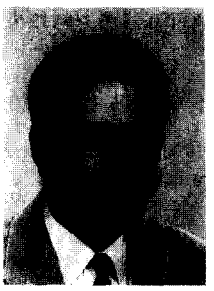

John Garratt, ARCS, BSc, DIC, PhD, spent seven years at Imperial College, University of London in the Departments of Physics and Meteorology before emigrating to Australia to take up a 3-year fellowship with CSIRO. He has been a research scientist at the CSIRO Division of Atmospheric Research since October 1970, and is currently leader of the Atmospheric Processes Programme. His career has included visiting appointments to the National Center for Atmospheric Research (1980–1981), Boulder, Colorado and to Colorado State University (1987–1988) in Fort Collins.

His current research interests include the representation of soil-canopy and boundary-layer cloud processes in numerical models, and the validation of numerical simulations (in general circulation models) of the surface energy and surface radiation budgets. Each year he gives a full lecture course on the atmospheric boundary layer to honours and postgraduate students in the Department of Mathematics, Monash University. Cambridge University Press published his book *The Atmopsheric Boundary Layer* in 1992 (softback in 1994).